Pcdh20 is a POU2F3 target gene required for proper tuft cell microvillus formation

Katherine E. Ankenbauer[1,2], Yilin Yang[1,2,3], Chi-Yeh Chung[4], Leonardo R. Andrade[5], Sammy Weiser Novak[6], Brenda Jarvis[1], Wahida H. Ali Hanel[4,7], Jiayue Liu[1], Victoria Sarkisian[1], Neil Dani[1], Evan Krystofiak[1], Gaizun Hu[8], Seham Ebrahim[8], Bechara Kachar[9], Qizhi Gong[10], Geoffrey M. Wahl[4], Uri Manor[11], Ken S. Lau[1-3,12-15] and Kathleen E. DelGiorno[1-3,13-16,*]

[1]Department of Cell and Developmental Biology, Vanderbilt University, Nashville, TN, USA
[2]Epithelial Biology Center, Vanderbilt University Medical Center, Nashville TN, USA
[3]Center for Computational Systems Biology, Vanderbilt University, Nashville TN, USA
[4]Gene Expression Laboratory, The Salk Institute for Biological Studies, La Jolla, CA, USA
[5]Laboratory of Genetics and Center for Chemical Biology and Proteomics, The Salk Institute for Biological Studies, La Jolla, CA, USA
[6]Waitt Advanced Biophotonics Center, Salk Institute for Biological Studies, La Jolla, CA, USA
[7]Biological and Physical Sciences Department, Columbus State Community College, Columbus, OH, USA
[8]Center for Membrane and Cell Physiology, Department of Molecular Physiology and Biological Physics, University of Virginia School of Medicine, Charlottesville, VA, USA
[9]Laboratory of Cell Structure and Dynamics, NIDCD, NIH, Bethesda, MD, USA
[10]Department of Cell Biology and Human Anatomy, School of Medicine, University of California, Davis, CA, USA
[11]Department of Cell and Developmental Biology, University of California, San Diego, CA, USA
[12]Chemical and Physical Biology Program, Vanderbilt University, Nashville TN, USA
[13]Department of Surgery, Vanderbilt University Medical Center, Nashville, TN, USA
[14]Vanderbilt Ingram Cancer Center, Vanderbilt University Medical Center, Nashville, TN, USA
[15]Vanderbilt Digestive Disease Research Center, Vanderbilt University Medical Center, Nashville, TN, USA
[16]Lead contact
* Correspondence: Kathleen.delgiorno@vanderbilt.edu

SUMMARY: (150 words)
Tuft cells are solitary chemosensory cells known for their distinct tall, blunt microvilli, thought to be analogous to mechanosensory hair cell stereocilia. Identification of commonalities between tuft and hair cells could identify a role for tuft cells in mechanotransduction. Transcription factor POU2F3 is the master regulator of tuft cell formation, however how POU2F3 drives formation of this unique cell and the functional role of the microvillar apparatus is unknown. POU2F3 ChIP-seq was performed on isolated tuft cells and compared to the cochlear hair cell transcriptome. Structural genes common to both tuft and hair cells, including protocadherin 20 (PCDH20), were identified. Immunogold labeling and imaging localized PCDH20 to extensive intermicrovillar linkages in tuft cells. Knockdown of PCDH20 in mice resulted in impaired microvilli formation and a disruption in structure. Altogether, PCDH20 is a POU2F3 target gene in tuft cells critical to maintain the rigid microvillar apparatus, which may function in mechanotransduction.

KEY WORDS:

Tuft cells; POU2F3; PCDH20; mechanotransduction; hair cells; microvilli; vesicles; ChIP-seq

INTRODUCTION:

Tuft cells are rare chemosensory cells found throughout the respiratory and digestive tracts that are analogous to taste cells. They are defined by their highly specific cytoskeletal structure of tall, blunt microvilli, thick, deep actin rootlets, and a well-developed tubulovesicular system that projects throughout the supranuclear cytoplasm[1]. Due to this unique structure, tuft cells have been identified by electron microscopy (EM) by many independent groups and received several names (e.g. fibrillovesicular, multivesicular, brush, caveolated cells) before more recent consensus settled on 'tuft cell'[1,2]. Despite characterization of this cell type as early as 1956[3], little functional data existed in the gastrointestinal tract until 2016 when three independent groups demonstrated that tuft cells function in the clearance of Helminth parasites in the intestines through the synthesis and secretion of cytokine IL-25[4-6]. Since then, tuft cells have been shown to sense the metabolite succinate in the intestine and trachea[7] and to secrete cysteinyl leukotrienes in response to *Alternaria* challenge in the tracheal and airway epithelium[8]. In the gallbladder, tuft cells also produce cysteinyl leukotrienes as well as acetylcholine (ACh), driving contraction and release of mucins, which may play a role in controlling tissue inflammation in response to commensal microbes[9,10]. In the pancreas, we have shown that tuft cells mitigate inflammation and inhibit tumorigenesis through eicosanoid prostaglandin D_2[11]. Despite these varied and context-specific functions, tuft cells in different organs and disease states all require transcription factor POU2F3 and share a well preserved structure, for which a functional role has yet to be demonstrated[12].

POU Class 2 Homeobox 3 (POU2F3, also known as SKN-1A or OCT11) is the master regulator transcription factor for tuft cell formation[13]. Full body POU2F3 knockout mice lack tuft cells in all organs as well as electrophysiological and behavioral responses to sweet, umami, and bitter compounds, due to a complete loss of sweet, umami, and bitter taste cells[14]. Like taste cells, tuft cells express the taste chemosensation pathway including G protein coupled taste receptors[15], which signal through GNAT3, PLCβ2, and ITPR3 to induce calcium flux, opening cation channel TRPM5; in taste cells this results in depolarization and secretion of ATP to adjacent nerves[16]. Outside of the tastebud, multiple studies have demonstrated that this machinery allows tuft cells to monitor intraluminal homeostasis, to achieve local responses to irritants, infection, or tumorigenesis via secreted effectors[17]. Unlike taste cells, tuft cells possess a distinct microvillus apparatus, currently without a known function.

Ultrastructural studies of murine gallbladder tuft cells show that, at a diameter of 0.18-0.2 μm, tuft cell microvilli are thicker than the conventional microvilli characteristic of intestinal enterocytes. Due to their stiff appearance, tuft cell microvilli, instead, more closely resemble the stereocilia of hair cells although not exhibiting the staircase morphology. Freeze fracture deep-etching replicas and electron microscopy (EM) studies are consistent with this assessment and led to the hypothesis that, like the stereocilia of hair cells, tuft cell microvilli may also function in mechanotransduction[2].

In the inner ear, the auditory and vestibular systems detect and translate sound waves and head positioning, respectively, by transforming mechanical input into electrical signal through specialized actin-filled microvilli

called stereocilia (organized in hair bundles). While the sensory inputs for hair cells are mechanical rather than chemical, the brain receives information electrically and, therefore, the process by which hair cell bundles transmit this physical information is called mechanoelectrical transduction. Displacement or deflection of the hair bundles through sound or movement causes tension on tip link filaments between stereocilia, which are composed of a dimer of cadherin 23 (CDH23) at the upper end of the tip link bound to a dimer of protocadherin 15 (PCDH15) at the lower end of the tip link. This tension opens a channel composed of transmembrane channel-like proteins 1 and 2 (TMC1, TMC2), located on the tips of shorter row stereocilia[18]. The resulting influx of Ca^{2+} and K^{+} ions depolarizes the hair cells and results in the secretion of neurotransmitters to afferent nerve fibers[19]. Disruption of stereocilia structure or this carefully controlled mechanotransduction signaling process often results in deafness or balance disorders; highlighting a critical way in which form follows function[18].

The structural similarities between tuft cell microvilli and hair cell stereocilia led us to ask if tuft cells express components of the mechanotransduction machinery and how POU2F3 regulates this process. Here, we performed POU2F3 chromatin immunoprecipitation sequencing (ChIP-seq) on isolated tuft cells and identified structural gene targets of POU2F3 that are shared with hair cells. Protocadherin 20 (PCDH20) was identified as a novel structural protein in both cell types and a likely component of intermicrovillar linkage in tuft cells. Genetic ablation of PCDH20 resulted in impaired microvilli formation and fewer secretory vesicles in tuft cells. Collectively, we have identified a critical tuft cell structural protein as a first step to understanding how this unique tuft cell structure dictates cell function.

MATERIALS AND METHODS:

Mice. Mice were housed in accordance with National Institutes of Health guidelines in American Association for Accreditation of Laboratory Animal Care-accredited facilities at the Salk Institute, the University of California San Diego, and the University of Virginia. The animal holding rooms were maintained at 70°F +/- 2 degrees. Animal rooms are pathogen free, excluding common endemic pathogens. Wild type male C57B6/J mice were purchased from Jackson Laboratories. *Pcdh20-/-* mice were generated using clustered regularly interspaced short palindromic repeats (CRISPR). The gRNA to the mouse PCDH20 gene and Cas9 mRNA were co-injected into fertilized mouse eggs to generate targeted knockout offspring. F0 founder animals were identified by PCR product sequence analysis and were confirmed by off-target analysis. PCDH20 knockdown mice were genotyped using the following primers which recognize both wild-type (374 base pairs) and mutant alleles (323 base pairs): mPCDH20-5b, 5'- GGA AGT TTA GCA TTG TCC CTG G- 3', mPCDH20-3b, 5'-GGT TGT TTA GGG TCA CAT ACT GG-3'.

Tuft cell preparation and isolation. Intestinal tuft cells were isolated as previously described[4,11]. The proximal 5 cm of the murine small intestine was first dissected, then flushed, cut longitudinally, and rinsed to remove luminal contents. Tissues were incubated in a 37°C shaker for 20 minutes, in 5 mL 1 x PBS containing 2.5 mmol/L EDTA, 0.75 mmol/L dithiothreitol, and 10 mg/mL DNAse I. Tissues were shaken vigorously for 30 seconds, large pieces of intestinal wall were removed, and cells were spun down at 4°C, 1200 revolutions/minute, for 5 minutes. Supernatant was removed, and cells were resuspended in 5 mL Hank's balanced salt solution with 1.0 U/mL dispase and 10mg/mL DNAse I, shaking for 10 minutes at 37°C. Digested cells were passed through a 100 μm filter and incubated with ACK lysing buffer. Single-cell suspensions were incubated on ice with mouse Fc receptor block (BD Biosciences, San Jose, CA; 1:200) followed by antigen-specific antibodies in FACS buffer. Then, 40,6-diamidino-2-phenylindole (Molecular Probes, Eugene, OR; 1:1000) was used to exclude dead cells. Cells were labeled with CD45 (Alexa Fluor 488), EpCAM (Alexa Fluor 647), and Siglec F (PE) (all BioLegend, 1:200). Fluorescence-minus-1 staining controls were included for gating populations of interest. Cells were FACS purified at the Salk Institute's Flow Cytometry core facility on a BD Biosciences Influx cell sorter (100 μm size nozzle, 1 x PBS sheath buffer, with sheath pressure set to 20 pounds/square inch) or an Aria Fusion cell sorter (BD Biosciences Billerica, MA). Cells were sorted in 1-drop single-cell sort mode for counting accuracy into DMEM + 10% FBS.

POU2F3 chromatin immunoprecipitation (ChIP) sequencing. Due to the low abundance of tuft cells in the murine small intestines (~0.4%)[4], we adapted a low input ChIP protocol called ChIPmentation with minor modifications[20]. Two pools of tuft cells from four adult male C57BL6/J mice were used as biological replicates. Approximately $1x10^4$ sorted tuft cells were crosslinked with 1% PFA at room temperature for 10 minutes, sonicated with Covaris M220 into 200-700 bp fragments, and incubated with 0.6 μg of anti-POU2F3 antibody (Santa Cruz #SC330) or control antibody (anti-IgG Cell Signaling #2729) overnight at 4°C. Protein A bead pull down (Invitrogen 10001D), washing, on-beads tagmentation (Illumina Nextera FC-121-1030), reverse crosslinking, library amplification (16-18 PCR cycles) and DNA purification were performed as

described. The input library was prepared by tagmentation of 1 ng of sonicated and reverse crosslinked mouse chromatin and then amplified and processed as the ChIP DNA. The control and ChIP samples were analyzed by Agilent TapeStation, and 50 bp single-end sequencing was performed with Illumina HiSeq 2500.

POU2F3 ChIP-seq analysis and comparison to hair cells. ChIP-seq data analyses were performed as previously described[21]. In brief, sequencing reads were checked by FastQC and aligned to mm9 with Bowtie (-k 1 -m 20 --best -S -n 2 -l 40)[22]. MACS2 (--nomodel --shift 100 --bw 150 --SPMR) was used to remove duplicated reads, call peaks and generate Bedgraph files that show fold change enrichment over input[23]. To ensure the quality of the POU2F3 binding sites, only peaks common between the two biological replicates (FDR<0.05) were called, and any peaks that overlap with the control IgG peaks (FDR<0.05) and the Encode blacklist regions were removed. Bedgraph files were then converted into BigWig files and uploaded to the UCSC Genome Browser for visualization. Signal profiling and correlation analysis were performed using deepTools [24]. Functional annotation of peaks and peak-gene association were done with GREAT (version 3.0.0) using the default "basal plus extension" parameter [25]. HOMER was used for motif enrichment analysis with size setting to 1000 bps [26]. Signals are visualized with trackplot R package (https://github.com/PoisonAlien/trackplot) for POU2F3 ChIP and IgG control across different gene regions.

Comparison to tuft cell and hair cell RNA-seq datasets. The differentially expressed genes in mouse inner hair cells (P20) from a publicly available dataset[27] were compared with POU2F3 ChIP-seq target genes. GO Enrichment Analysis was performed on the overlapping gene set using the enrichGO function from the clusterProfiler R package (https://github.com/YuLab-SMU/clusterProfiler).

Computational Analysis of RNA-seq datasets. Single-cell RNA sequencing (scRNA-seq) data generated from gallbladder and extrahepatic duct tissue from *Pou2f3+/+* and *Pou2f3-/-* mice[10] (GEO accession: GSE194035) were obtained from the GEO database in filtered_feature_bc_matrix.h5 format. Data processing was performed using the Seurat V5.1[28] in R. For quality control, only cells with a minimum of 200 detected genes and present in at least 3 cells were preserved. Cells were then filtered to retain those with 300–5000 features, <20,000 RNA counts, <15% mitochondrial genes, and <0.1% hemoglobin expression. Following QC, the datasets were merged. Data normalization and variance stabilization were then performed using SCTransform while regressing out mitochondrial gene expression. Dimensionality reduction was achieved via principal component analysis (PCA), and cell-to-cell distances were computed using FindNeighbors (dims 1:50). Unsupervised clustering was performed with a resolution of 0.6 (with 30 starts), followed by Uniform Manifold Approximation and Projection (UMAP) for visualization of the cellular landscape. Feature plots for selected genes of interest (including *Pcdh20*, *Whrn*, *Espn*, and *Clic5*) were generated using Featureplot() based on orig.ident and arranged in a combined layout for comparison between the two genotypes.

Fluorescence Microscopy. Fluorescence microscopy was performed as previously described[11,29]. Briefly, tissues were fixed overnight in 4% paraformaldehyde, washed 3 times with PBS, and floated overnight in 30% sucrose at 4°C. Tissues were then incubated in a 1:1 mixture of 30% sucrose and Tissue-Tek optimal

cutting temperature compound (OCT) (VWR, Radnor, PA) for 30 minutes, embedded in OCT, and frozen at -80°C. 7-10 μm tissue sections were cut, permeabilized with 0.1% Triton X-100 in 1x PBS, and blocked with 5% normal donkey serum and 1% BSA in PBS for 1 hour at room temperature. Tissue sections were stained with primary antibodies (Table S1) in 1 x PBS supplemented with 1% BSA and 0.1% Triton X-100 overnight. In some experiments, a polyclonal antibody against PCDH20, made against C-terminal amino acid 940-952, CMRERKPVDISNI, of the mouse protein (AB_3676540) was used[30]. Sections were then washed for 3 x 15 minutes in PBS with 1% Triton X-100, incubated with Alexa Fluor secondary antibodies and/or phalloidin (Invitrogen, Waltham, MA), washed again for 3 x 5 minutes, rinsed with distilled water, and mounted with Prolong Gold containing 4',6-diamidino-2-phenylindole (Thermo Fisher). Tissues were imaged on either a Zeiss (Oberkochen, Germany) 710 confocal microscope, a Zeiss 880 or 980 Airyscan Super-Resolution microscope, an Andor BC43, or a Leica (Wetzlar, Germany) MICA confocal microscope using an HC PL APO 20x/0.75 or HC PL APO 63x/1.20 W objective.

Whole Mount Immunofluorescence. Tissues were dissected from wild-type mice immediately after euthanasia and cut into 0.5 cm X 0.5 cm squares. Tissues were fixed in 4 % PFA in PBS for 1 hour before washing in PBS 3 x 15 minutes. Tissues were then incubated 1:1000 Alexa Fluor 405 Phalloidin in 0.5 % PBST for 30 minutes, before washing in PBS for 15 minutes. Tissues were blocked by incubating in 10% NGS for 4 hours, before incubating in 1:400 primary antibody overnight at 4 C. Tissues were then washed again in PBS 3 x 15 minutes before incubating in 1:1000 anti-rabbit secondary antibody for 1 hour. Finally, tissues were washed again in PBS 3 x 15 minutes before mounting on slides with ProLong Gold antifade mounting media. TMC1 images were captured on a Nikon ECLIPSE Ti2-E inverted microscope with Yokogawa CSU-W1 Spinning Disk and Hamamatsu ORCA-Fusion BT Digital CMOS camera C15440-20UP.

PCDH20 Transfection. HeLa or U2OS cells were passaged in DMEM supplemented with 10% FBS and 100 μg/mL penicillin-streptomycin and were split at a ratio of 1:10 once every two to three days using Trypsin. At 80% confluency, cells were transfected with either GFP or PCDH20-GFP (generated by the Gong Laboratory). 3.7 μg of PCDH20 plasmid was diluted 1:1000 in OptiMeM and cells were transfected using Lipofectamine for 48 hrs. Cells were then washed and fixed with paraformaldehyde, stained, and imaged as previously described.

Scanning Electron Microscopy (SEM). SEM was performed as previously described[12,29]. Briefly, small intestines or gallbladders from wild-type or PCDH20 knockdown C57Bl6/J mice were freshly dissected, cut into 2-mm fragments and immediately fixed with 4% formaldehyde, 2.5% glutaraldehyde, 0.1M sodium cacodylate buffer (pH 7.2), and 2mM CaCl2 for 2 hours at room temperature. Samples were then washed for 3 x 15 minutes in the same buffer and incubated with 2 consecutive baths of 1% osmium tetroxide and 1% tannic acid for 1 hour each with 3 x 10-minute water washes in between each bath. Samples were dehydrated in a graded series of ethanols until absolute and critical point dried (Leica CPD300, Wetzlar, Germany). All reagents were bought from Electron Microscopy Sciences, Hatfield, PA. They were then mounted on carbon tape covering aluminum stubs and sputtered coated with platinum (4 nm) (Leica EM

SCD500). Tissues were imaged on a FEG-SEM Zeiss Sigma VP, operated at 5 kV, and were photographed at 2048 x 1536 pixels of resolution. **SEM Analysis.** SEM images were analyzed using FIJI[31] and Graphpad Prism. Briefly, scale was set for each individual image, and an ROI was manually drawn to determine tuft cell microvilli size. Microvillar angles were measured on tuft projections with FIJI's angle tool. Vesicles were drawn manually on all microvillar projections in each tuft; ROIs were filled in and quantified using the Analyze Particles function. Data was compiled into Prism Graphpad for visualization and statistical analysis.

Scanning EM of ultrathin sections. Murine small intestines was processed and imaged as described previously with some modifications[32]. Materials were sourced from Electron Microscopy Sciences (Hatfield, PA) unless noted otherwise. Briefly, fresh biopsies of small intestines were dissected into small pieces (<1 mm) and quickly immersed in 37°C buffered fixative (2.5% glutaraldehyde, 2% paraformaldehyde, 3 mM CaCl2, 0.1M sodium cacodylate) before overnight storage at 4°C in the same solution[33]. Samples were serially rinsed with ice-cold cacodylate/CaCl2 buffer and stained with buffered reduced osmium (1.5% Osmium, 1.5% potassium ferrocyanide, 3 mM CaCl2, 0.1M sodium cacodylate) for 45 minutes in the dark at room temperature. Samples were serially rinsed with ice-cold distilled water before 30 minutes of treatment with filtered 1% aqueous thiocarbohydrazide (Ted Pella, Redding, CA) that was prepared at 60°C for an hour before use. Samples were serially rinsed with ice-cold distilled water before staining with 1.5% aqueous osmium tetroxide for 45 minutes in the dark at room temperature. Samples were rinsed serially with ice-cold water before staining overnight with 1% uranyl acetate at 4°C. Samples were then rinsed with distilled water and stained with Walton's lead aspartate for 30 minutes at 60°C[34]. Samples were rinsed again with distilled water and serially dehydrated in ice cold ethanol. Samples were then infiltrated with Durcupan resin (hard formulation) and polymerized at 60°C for 3 days. A sample block was prepared for serial sectioning as previously described and a ribbon of 248 serial sections, each of dimension ~150 μm x 400 μm x 70 nm (x-y-z), were collected onto a silicon wafer diced to a dimension of 35 x 6 mm using Diatome diamond knives mounted in a Leica UC8 ultramicrotome[35]. The chip was imaged using a Zeiss Sigma VP scanning electron microscope equipped with a Gatan backscattered electron detector and Atlas5 (Fibics) control software. Images were collected at a working distance of between 4-5mm and with an accelerating voltage of 3kV and pixel sizes between 2-8nm.

Transmission Electron Microscopy Freeze Substitution Protocol. Gallbladder was fixed in 0.5% glutaraldehyde, 4% paraformaldehyde in 0.1 M sodium cacodylate for 1 hour then gradually cryoprotected to a final concentration of 30% glycerol in 50 mM HEPES. Samples were plunge frozen in liquid ethane. Frozen samples were freeze-substituted in a Leica Biosystems AFS2 with 1.5% uranyl acetate in absolute methanol at -90°C for 2 days, then infiltrated with HM20 Lowicryl resin (Electron Microscopy Sciences) over the course of 2 days at -45°C. Finally, the resin was UV-polymerized for 2 days between -45°C and 0°C. Ultrathin sections (70 to 100 nm) were cut and collected on 300-mesh Ni grids (Electron Microscopy Sciences). Grids were post-stained with 2% uranyl acetate and lead citrate. Samples were imaged on a 200-a JEOL 2100 Plus at 200 keV equipped with an AMT nanosprint15mkII CMOS camera; processing was done with FIJI and was limited to cropping and linear adjustments to brightness and contrast.

Freeze fracture and etching Electron Microscopy (FFE-EM). Preparation of fixed samples: Samples were incubated with 2% glutaraldehyde overnight and then washed in ddH_2O. Fixed samples were then fast frozen using a Life Cell CF-100 slam-freezing machine. Frozen tissue was subjected to freeze-fracture at -110°C in a Balzers freeze-fracture machine, followed by freeze-etch at -100°C for 10 min. Freeze-etched samples were rotary shadowed with platinum and stabilized with carbon using electron-beam metal-evaporation guns (Cressington Scientific) to create replicas of the exposed surfaces. Replicas were cleaned with sodium hypochlorite, washed with ddH_2O, and transferred onto 300 mesh hexagonal copper grids (Electron Microscopy Sciences). Replicas were imaged on a JEOL 2100 transmission electron microscope with an Orius 832 CCD camera (Gatan). Images were captured with DigitalMicrograph (Gatan).

Immunogold Labeling and Imaging. Immunogold labeling was done similar to previously described[36]. In brief, samples were antigen retrieved using 0.1% sodium borohydride, 50 mM glycine in tris buffered salt solution (TBST, 5 mM Tris, 0.81% NaCl, 0.1% Triton X-100) for 10 minutes followed by blocking in 10% normal goat serum in TBST for 30 minutes. Samples were stained with primary antibody (PCDH20, Gong Laboratory) at a dilution of 1:100 in TBST with 1% normal goat serum for 1 hour. Samples were extensively washed in TBST with 1% normal goat serum and then stained with 10 nm colloidal gold conjugated to goat anti-chicken secondary (Electron Microscopy Sciences) for 1 hour. Samples were washed in TBST, followed by ddH_2O. Grids were post stained with 2% uranyl acetate. Immuogold labeled samples were imaged on a JEOL 2100 Plus transmission electron microscope with an AMT nanosprint15mkII camera using SerialEM to acquire the images.

Statistical Analysis. Statistical analyses and data processing were performed in Image J or Graphpad Prism (GraphPad, San Diego, CA). Statistical significance was calculated by either 2-tailed unpaired t-tests assuming equal variance or 1-way analysis of variance. Data are expressed as mean ± standard deviation. Figures were generated with Adobe Photoshop and Illustrator. Figure 7 was generated with bioRender.

RESULTS:

ChIP-seq identifies POU2F3 target genes in tuft cells. Transcription factor POU2F3 is the master regulator of tuft cell formation in normal organs, as well as for those forming *de novo* in disease, such as in pancreatic tumorigenesis[4,11,37,38]. POU2F3 is known to function in taste sensation and keratinocyte maturation[14,39], however little is known about POU2F3 target genes in normal cells or how tuft cell formation is regulated. To identify targets of POU2F3 binding, we performed chromatin immunoprecipitation sequencing (ChIP-seq) on isolated small intestinal tuft cells. Tuft cells make up only ~0.4% of the epithelium in the murine small intestines[4]. Therefore, to acquire the requisite 10,000 cells needed for this analysis, we sorted large portions of normal duodenum from multiple adult mice and pooled samples. Tuft cells were isolated and concentrated by fluorescence activated cell sorting (FACS) using a Siglec F^+;$EpCAM^+$ signature, as previously described[4,11,29]. Duplicate POU2F3 ChIP-Seq libraries were prepared from two independent experiments and compared to an untargeted IgG binding control (**Figure 1A**). Q enrichment score (QES) analysis was performed to verify the quality of these POU2F3 binding sites. Only peaks (FDR < 0.05) common between the two biological replicates were called and any that overlapped with the IgG control and/or ENCODE blacklist regions were removed. Compared with the reference values for the quality metrics generated from 392 data sets from ENCODE, the QES from our POU2F3 ChIP-seq was ranked at the level of moderate high to very high, suggesting high quality POU2F3 peaks.

Next, the distribution of peaks across functional domains in the genome was analyzed. POU2F3 peaks were strongly enriched in gene-associated functional domains, such as promoter (defined as -1 kb to +100 bp of transcription start site, 14.27%), un-translated region (2.45%), intron (36.31%), and exon (4.43%), where they usually mapped within 1kb of the TSS, indicating that the peaks generated from our POU2F3 ChIP-seq were not located randomly on the genome but instead were associated with core promoters (**Figure 1B, S1A**). To identify direct POU2F3 transcriptional targets, we defined genes that have POU2F3 binding sites as proximal, 5 kb upstream or 1kb downstream of the TSS, or distal, up to 1000 kb, as POU2F3-associated genes. We identified a total of 2828 POU2F3 high confidence binding regions which were mapped to 3032 genes across all 21 genomic chromosomes (**Figure S1B**).

Next, we performed *de novo* motif analysis for our POU2F3 ChIP-seq data using HOMER. As expected, POU2F3 bound chromatin was significantly enriched for the consensus POU motif ($p < 1 \times 10^{-945}$), demonstrating that direct binding sites for POU transcription factors are enriched in our ChIP-seq data (**Figure 1C**). Interestingly, the consensus DNA binding motifs of several transcription factors highly expressed in tuft cells matched binding sequences derived *de novo* from POU2F3 ChIP-seq analysis. Included are *Ehf* (EHF, $p < 1 \times 10^{-39}$)[40], *Runx1* (RUNX, $p < 1 \times 10^{-36}$), and *Sox9* (SOX, $p < 1 \times 10^{-24}$)[41], suggesting the possibility that these factors bind cooperatively with POU2F3 to regulate tuft cell formation (**Figure 1C**)[11].

To identify direct POU2F3 transcriptional targets in tuft cells, we compared our new POU2F3 ChIP-seq analysis with a previous messenger RNA (mRNA)-based dataset we generated using SmartSeq2 on low

abundance samples where we identified 819 significantly upregulated and 900 significantly downregulated genes in tuft cells as compared to non-tuft epithelial cells in the duodenum[11]. When comparing the two datasets, we identified significant overlap of POU2F3 ChIP-seq target genes and the tuft cell transcriptomic signature (43%, $p = 2.16 \times 10^{-23}$), consistent with a role for POU2F3 in specifying tuft cell fate. Many POU2F3 target genes serve as canonical tuft cell markers, including *Trpm5*, *Chat*, *Ptgs1*, *Il25*, *Spib*, and *Pou2f3* itself (**Figure 1D, File S1**). Additional genes common to both datasets include *Alox5*, *Bmp2*, *Cd300lf*, *Dclk1*, *Gnat3*, *Hpgds*, *Sucnr1*, *Vav1*, and many others previously described to be enriched in tuft cells (**Figure 1E**, **File S2**)[11]. POU2F3 expression has also been described in a variant of human non-small cell lung cancer (NSCLC) expressing tuft cell markers[42]. To compare POU2F3 target genes between species and disease states, we compared our POU2F3 ChIP-seq dataset to one generated in a tuft cell-like human NSCLC cell line[42]. Interestingly, we found that 70.4% (2136/3032) of POU2F3 ChIP target genes identified in murine tuft cells overlapped with the human dataset, which also included *ALOX5*, *BMP2*, *DCLK1*, *GNAT3*, *HPGDS*, *SUCNR1*, and *VAV1*, consistent with a role for POU2F3 in driving a tuft-like fate (**Figure 1F**, **File S3**).

To gain broader insight into POU2F3 target genes, Genomic Regions Enrichment of Annotations (GREAT) analysis was performed on our POU2F3 ChIP-seq dataset. Here we identified immune cell signaling pathways such as 'B cell receptor signaling pathway', 'B cell activation', 'Members of the BCR signaling pathway', and 'T cell activation'. Lipid metabolism pathways, including 'Fatty acid alpha-oxidation' and 'Biosynthesis of prostaglandins', were identified, consistent with a known role for tuft cells in eicosanoid synthesis[11]. Finally, we identified several pathways consistent with a possible role for tuft cells in microbial interactions, including 'Cellular response to lipopolysaccharide', 'Cellular response to molecule of bacterial origin', and 'Cellular response to biotic stimulus' (**Figure 1G**). Gene Ontology (GO) pathway analysis of genes common to both our ChIP-seq and RNA-seq datasets again identified immune cell signaling pathways such as 'B cell receptor signaling pathway' and 'Regulation of B cell receptor signaling pathway' and eicosanoid biosynthesis pathways such as 'Synthesis of lipoxins' (**Figure S2**). Collectively, these analyses identified genes in tuft cells putatively regulated by POU2F3. Significant overlap between ChIP target genes and mRNA enriched in tuft cells identifies direct POU2F3 target genes and a mechanism by which POU2F3 drives tuft cell fate.

POU2F3 ChIP-seq reveals a cochlear hair cell gene signature. Tuft cells are identified by their distinct cytoskeletal structure of tall, blunt microvilli and deep actin rootlets (**Figure 2A**). Among POU2F3 target genes in our ChIP-seq analysis, we identified several encoding known tuft cell structural proteins including *Avil*[43], *Cdhr2* and *Cdhr5*[44], and *Krt18* and *Vil1*[45] (**File S1**). These data suggest that POU2F3 activity is required for assembly of the microvillus/rootlet apparatus. Freeze fracture electron microscopy studies of murine gallbladder tuft cells suggest that tuft cell microvilli are more similar to cochlear hair cell stereocilia than the conventional microvilli characteristic of intestinal enterocytes[2]. Based on size and ultrastructural features suggesting stiffness, these data indicate a possible role for tuft cell microvilli in mechanotransduction. To identify commonalities between tuft cells and cochlear hair cells, a prototypical mechanosensory cell type, we compared our POU2F3 ChIP-seq dataset to a single cell RNA-seq (scRNA-seq) dataset generated from adult murine cochlea[27]. As shown in **Figure 2B**, we found that 27.2% (825/3032)

of ChIP-seq target genes overlapped with the inner hair cell transcriptomic signature. Mutations in many of these genes, including *Grxcr1*[46], *Cldn14*[47], and *Myo6*[48] are associated with deafness, highlighting their critical role in hair cell function (**Figure 2C, S3**).

Among genes common to both our tuft cell POU2F3 ChIP-seq and the outer hair cell transcriptome, we identified *Espn*, which is an actin cytoskeletal regulatory protein that contributes to the integrity of parallel actin bundles in the microvilli and stereocilia of chemosensory and mechanosensory cells[49,50]. *Clic5*, a member of the chloride intracellular channel protein family, is required for stereocilia formation in the inner ear and normal hearing[51-53]. The gene *Whrn*, encoding Whirlin, is necessary for elongation and maintenance of inner and outer hair cell stereocilia in the organ of Corti and defects are also associated with deafness[54]. *Tmc1* is a pore-forming member of the mechanotransducer (MET) non-selective cation channel complex located at the tips of stereocilia that mediates sensory transduction. Loss or mutation also results in deafness by disturbing induction of the tension-induced MET channel and downstream signaling[55]. Finally, we identified *Pcdh20*, or protocadherin 20; expression of which has not been previously described in either tuft or hair cells (**Figure 2D**). Protocadherins are integral membrane proteins that mediate calcium-dependent cell-cell adhesion and are important components of the MET complex in the stereocilia of hair cells. While functional data on the role of PCDH20 in cochlear hair cells is lacking, genome-wide association analysis (GWAS) on normal hearing function (hearing thresholds and pure-tone averages) in populations in Italy, Central Asia, the United Kingdom, and Finland identified significant loci close to *PCDH20* as candidates for progressive hearing function and loss[56]. Interestingly, we also identified *ESPN*, *CLIC5*, *WHRN*, *TMC1*, and *PCDH20* as POU2F3 gene targets in the ChIP-seq study performed on the tuft cell-like human NSCLC cell line (**File S3**)[42].

To gain deeper insight into features shared between tuft and hair cells, and to identify a possible role for tuft cells in mechanotransduction, we performed GO analysis on the 825 genes shared between our POU2F3 ChIP-seq analysis and the adult inner hair cell transcriptome. Cytoskeletal pathways identified included 'cilium organization', 'actin filament organization', 'actin filament polarization', and 'stereocilium'. Similarities in cell type formation include 'inner ear development', 'inner ear morphogenesis', and 'inner ear auditory receptor cell differentiation'. Finally, similarities in function between tuft cells and hair cells are suggested by the terms 'sensory perception of mechanical stimulus', 'stimulus involved in sensory perception', and 'detection of mechanical stimulus involved in sensory perception of sound' (**Figure 2E, File S4**). Collectively, these data suggest that POU2F3 in tuft cells controls transcription of genes known to be involved in stereocilia formation and function.

PCDH20 is a tuft cell-specific protocadherin in the gut epithelium. To evaluate broad expression of identified cochlear hair cell genes in diverse tuft cell populations, we first analyzed several publicly available RNA-seq datasets. In a study conducted by Nadjsombati et al., normal tuft cell populations derived from murine small intestines, colon, gallbladder, thymus, and trachea were concentrated by FACS using an IL-25 fluorescent reporter mouse model and underwent bulk RNA-sequencing[7]. As shown in the principal

component analysis (PCA) in **Figure 3A**, tuft cell populations clustered by tissue type. *Espn* and *Clic5* expression were found to be significantly elevated in tuft cells as compared to non-tuft epithelial populations in the small intestines and were highly expressed in all tuft cell populations from all organs assayed. *Pcdh20* expression was absent from non-tuft intestinal cells but was identified at varying levels of expression in all tuft cell populations (**Figure 3B**). *Whrn* was expressed at very low levels and *Tmc1* was not identified (data not shown).

Next, we analyzed bulk RNA-seq datasets generated from metaplasia-derived, disease associated tuft cells. Here, DelGiorno et al., isolated tuft cells using the FACS strategy of collecting Siglec F^+ $EpCAM^+$ populations from the pancreas of mice with either chronic pancreatitis or oncogenic *Kras*^{G12D}-induced neoplasia[11,29]. As shown in **Figure 3C**, tuft cell populations clustered by disease state, however pancreas-derived tuft cells clustered more closely to each other than to normal duodenal tuft cells. In these datasets, *Espn* expression was significantly higher in tuft cells, as compared to non-tuft epithelial cells in both disease states, consistent with expression patterns identified in **Figure 3B**. *Clic5* expression was found to be significantly enriched in pancreas-derived tuft cells as compared to non-tuft cells; expression was present in this duodenal tuft cell dataset but was not significantly elevated. Finally, we assayed for *Pcdh20* expression and identified tuft cell-specific expression in all datasets (**Figure 3D**). Again, *Whrn* and *Tmc1* were not detected (data not shown).

Finally, we evaluated expression of cochlear hair cell genes in several scRNA-seq datasets. In O'Leary et al., authors performed scRNA-seq on gallbladders derived from wild type control mice or from *Pou2f3-/-* mice, which cannot form tuft cells (**Figure 3E**)[4,37]. As shown in **Figure 3F**, expression of *Espn*, *Clic5*, and *Pcdh20* were all found in tuft cells with *Espn* and *Pcdh20* expression largely lost in *Pou2f3-/-* mice. Again, *Whrn* and *Tmc1* expression was not identified (**Figure S4A**). Similar results were obtained in a scRNA-seq dataset of murine pancreatitis tuft cells (**Figure S4B**). Altogether, these data identify expression of several cochlear hair cell genes at the mRNA level in tuft cells with *Pcdh20* being largely tuft cell specific in the gut epithelium.

PCDH20 is enriched in tuft cell microvilli. To validate expression of cochlear hair cell markers at the protein level in tuft cells, we performed immunostaining in both the murine gallbladder and small intestines. Tuft cells were identified in both tissues by F-actin staining which labels the tuft cell microvilli and deep actin rootlets characteristic of this cell type, as in previous studies[29,57]. Consistent with previous work in the small intestines, Espin (*Espn*) was identified in tuft cells. We show here that Espin is expressed in gallbladder tuft cells as well and that expression largely overlaps with F-actin, consistent with a role in actin bundling (**Figure 4A-B**)[58]. Next, we evaluated PCDH20 expression in tuft cells by immunostaining. To validate PCDH20 antibody specificity, we generated controls by transfecting U2OS and HeLa cells with either a GFP or a PCDH20-GFP construct and performed immunostaining for PCDH20 (**Figure S5A-H**). Once PCDH20 expression was confirmed only in PCDH20-GFP transfected cells, we performed immunofluorescence on duodenal, gallbladder, and *Kras*^{G12D}-induced neoplastic pancreas tuft cells. In all tuft cell populations, PCDH20 localized to the apical microvilli, indicating a possible role in intermicrovillar linkage (**Figure 4C-D, S5I-L**).

Finally, we examined tuft cells for expression of Whrn and TMC1, which were identified in our ChIP-seq analysis, but were not detected in our analysis of published RNA-seq datasets. Whrn was identified in gallbladder, but not intestinal tuft cells, with expression enriched in the microvilli (**Figure S6**). Interestingly, expression of TMC1, a member of the MET complex that mediates sensory transduction in the hair cells, was identified in the microvilli of both gallbladder and intestinal tuft cells (**Figure 4E-F**). Collectively, these analyses confirm expression of cochlear hair cell markers in tuft cells, localizing several to the microvillar apparatus.

Tuft cells are characterized by extensive intermicrovillar linkages. In cochlear hair cells, stereocilia are connected by tip links, or small filaments required for the transmission of mechanical signals and hearing. These tip links are constructed of two proteins, cadherin 23 and protocadherin 15 (PCDH15). Loss of either results in deafness in murine models. Rather than cadherin 23, tuft cells have been shown to express CDHR2 (PCDH24) and 5, leading us to ask whether PCDH20 could play an analogous role to PCDH15 in tuft cells[44].

To determine whether tuft cells are characterized by intermicrovillar links, we performed several orthogonal EM techniques to resolve these structures in both the murine intestines and gallbladder. In the gallbladder, we performed both scanning electron microscopy (SEM) and transmission electron microscopy (TEM). We identified intermicrovillar links by SEM (**Figure 5A-C**), as well as TEM (**Figure 5D**), which also revealed links between tuft cells and neighboring epithelial cells (**Figure 5E**). In the small intestines, we found that the glycocalyx made these structures difficult to resolve by SEM (**Figure 5F-H**). To resolve this issue, we took a higher resolution approach and performed Freeze fracture deep etching electron microscopy (FFE-EM), which led to the discovery that the tuft cell microvillar apparatus is characterized by extensive linkage between individual microvilli, consistent with a predicted rigidity attributed to the structure (**Figure 5I-J**). Collectively, these analyses reveal intermicrovillar linkage in tuft cells which may contribute a lack of deflection or mobility, as occurs in hair cells, which could function in mechanotransduction by regulating a MET-like complex.

PCDH20 loss impairs tuft cell microvillar formation. By immunostaining, we identified PCDH20 expression in tuft cell microvilli, and our EM analyses revealed extensive intermicrovillar linkages in intestinal and gallbladder tuft cells (**Figures 4-5**). To determine if PCDH20 localizes to microvilli in a pattern consistent with lateral linkage, we performed EM immunogold staining. As shown in **Figure 6A**, PCDH20 localized to tuft microvilli, consistent with immunostaining. To determine if PCDH20 plays a functional role in the formation of these structures we generated a genetically engineered mouse model (GEMM) of PCDH20 loss using clustered regularly interspaced short palindromic repeats (CRISPR). Multiple founder mice were generated and screened for PCDH20 loss by DNA sequencing (**Figure S7**) and polymerase chain reaction (**Figure S8A**). Ultimately, we chose to further assay a mouse with a 121 base pair deletion and an 11 base pair insertion in exon 3 of *Pcdh20* (**Figure S7**). Loss of PCDH20 expression in *Pcdh20-/-* tuft cell microvilli

was confirmed by immunostaining intestinal tuft cells (**Figure 6B**). Ultrastructural analyses were further pursued in the gallbladder due to the high density of tuft cells in this organ as compared to the intestines.

By SEM analysis, gallbladder tuft cells in wild-type (*Pcdh20*+/+) mice were characterized by the tall, rigid microvilli previously described for this cell type (**Figure 6C**). In contrast, we found that the tuft cell microvilli in the *Pcdh20-/-* model were stunted in size and hung from the center of the cell giving them an almost irregular shape and appearance (**Figure 6D-E, Figure S8B-D**). In comparison to *Pcdh20*+/+ gallbladder tuft cells, the *Pcdh20-/-* tuft cell microvillar apparatus was found to be smaller (1.6×10^7 nm^2, 50 tuft cells vs 0.6×10^7 nm^2, 25 tuft cells, $p < 0.05$) and to contain fewer microvilli (~212 microvilli, 13 tuft cells vs. 159 microvilli, 19 tuft cells, $p < 0.05$) (**Figure 6F-G**). *Pcdh20*+/+ microvilli were found to be straighter, or more vertical, and closer to a 180° angle than those in *Pcdh20-/-* (172.5°, 13 tuft cells vs. 166.8°, 19 tuft cells, $p < 0.01$) (**Figure 6H**). Analysis of the vesicles budding from microvilli revealed significantly less in the *Pcdh20-/-* model (206 vesicles, 13 tuft cells vs. 114 vesicles, 19 tuft cells, $p < 0.05$) (**Figure 6I**). This, however, is likely due to the smaller number of microvilli in *Pcdh20-/-* tuft cells as the average number vesicles per microvillus was unchanged (**Figure 6J**). The size of the vesicles, consistent with smaller tuft cells size, was found to be smaller in *Pcdh20-/-* tuft cells as compared to control (2.7×10^3 nm^2, 13 tuft cells, vs. 1.5×10^3 nm^2, 19 tuft cells, $p < 0.01$) (**Figure 6K**). Altogether, these data demonstrate that PCDH20 is a critical tuft cell structural protein, regulated by the lineage defining transcription factor POU2F3, that functions in the development of microvillar apparatus.

DISCUSSION

Tuft cells are identified by their striking morphology; however, how form follows function for this cell type has yet to be determined. Though still a relatively young field, tuft cell biologists have identified roles for tuft cells in several disease states including infection (parasite, bacterial, viral), tissue injury, inflammation, and tumorigenesis[12] A role for chemosensation has been demonstrated in several of these states, however whether tuft cells signal via mechanotransduction has not yet been examined. Microvilli enhance membrane surface area, playing a role in absorption in enterocytes, however specialized microvilli, such as stereocilia are required for critical mechanotransduction processes, such as in hearing and balance[19]. Here, we showed that tuft cells share several structural elements with cochlear hair cells. We identified common gene expression signatures including actin bundling, stereocilium assembly, and sensory perception of mechanical stimulus (**Figure 2E**). Interestingly, these data suggest that many targeted mutations resulting in deafness may also cause dysfunctional tuft cell formation, perhaps resulting in respiratory or digestive issues, or an impaired ability to heal from infection or tissue injury.

Among genes common to both our POU2F3 ChIP-seq analysis in tuft cells and the inner hair cell transcriptome, was *Pcdh20*. In hair cells, mechanoelectrical transduction is dependent on tip link proteins between stereocilia composed of PCDH15 and CDH23[19]. Based on our immunostaining and immunogold labeling studies, we hypothesize that PCDH20 plays a similar role in tuft cells, binding to CDHR5 to form intermicrovillar linkages (**Figure 7**). Whether PCDH20 directly binds CDHR5 or also interacts with CDHR2 has yet to be determined. Additional genes identified include several actin binding proteins, such as Espin, and other proteins involved in stereocilia elongation such as Whirlin, which are likely required to build the thick actin bundles characteristic of both cell types. TMC1 – a major component of the hair cell stereocilia mechanotransduction channel - was identified in both the tuft cell and lung cancer cell POU2F3 ChIP-seq analyses, as well as in tuft cells at the protein level. TMC1 expression could indicate the presence of a tuft cell MET-like complex. Other possible MET components expressed at the mRNA level in tuft cells, but not regulated by POU2F3, include TMC4/5 and CIB2, which were recently described in intestinal enterocytes[59]. It is likely, though, that tuft cells will form complexes constructed of analogous, yet unique protein components as compared to other cell types.

Consistent with a role in intermicrovillar linkage, loss of PCDH20 resulted in abnormal tuft cell microvilli with a markedly splayed appearance in comparison to the normally tight bundle of microvilli in WT cells. We found gallbladder tuft cells in *PCDH20-/-* to have smaller tufts with irregular microvilli and fewer apical vesicles. These data suggest that loss of PCDH20 may interfere with apical tuft cell secretion. Loss of PCDH20 also significantly impacted the rigidity and perceived stiffness of the microvilli bundles. This may impact mechanotransduction in several ways: 1. By removing intermicrovillar linkages required to open TMC channels and 2. By influencing the amount of force sensed by the now stunted and/or collapsed microvilli. In the gallbladder, which changes dramatically in size based on an organism's fed/fasted state, tuft cells may sense filling of the structure (during fasting), placing an applied force directly on the tuft. This could result in the release of known biliary tuft cell effectors, such as ACh and leukotrienes[9], to induce protective mucus release, thereby safeguarding against increasingly concentrated bile acids which are cytotoxic, and

tonic gallbladder contraction which prevents bile stasis. In the intestines, tuft cells are subjected to luminal forces, which may include both applied force (filling, parasite infection) and a parallel, tensional force which would displace microvilli, resulting in release of multiple effectors (e.g. acetyl choline, IL-25). We hypothesize that loss of PCDH20 reduces the ability of tuft cells to sense these forces. Future experiments will focus on both *in vitro* studies to measure tuft cell microvillar stiffness and the ability to directly sense different kinds of force and *in vivo* studies to determine how PCDH20 loss impacts tuft cell function in the contexts of homeostasis and disease.

Our ChIP-seq analysis revealed that many of these structural proteins, including *Pcdh20*, are regulated by transcription factor POU2F3. This is consistent with the role of POU2F3 as a master regulator for tuft cell formation, dictating tuft cell fate, in part, by directing formation of the unique structure. Many canonical tuft cell markers were identified in our analysis (e.g. *Il25*, *Ptgs1*, *Trpm5*, etc.) suggesting that POU2F3 directly drives expression of these genes. Interestingly, we also identified several neuronal genes in our ChIP-seq analysis. While many (e.g. Dclk1) have been described in tuft cells, it has also been shown that tuft and enteroendocrine cells are closely related in the intestines and diseased pancreas[60-63]. Loss of POU2F3 significantly increases abundance of enteroendocrine cells in pancreatic tumorigenesis suggesting that it not only drives expression of tuft cell genes but may also inhibit enteroendocrine-specific genes during tuft cell formation[64]. Future studies will focus on how POU2F3 both positively and negatively regulates tuft cell fate and identifying any critical binding partners (SOX9, RUNX1, etc.)

Altogether, this study identifies PCDH20 as a POU2F3 target gene and critical structural protein in tuft cells. To our knowledge, this is the first study demonstrating impaired tuft cell formation in response to structural protein loss. These data will serve as foundation for future studies on structure-function relationships in tuft cells.

RESOURCE AVAILABILITY

Lead contact

Further information and requests for resources and reagents should be directed to and will be fulfilled by the lead contact, Kathleen E. DelGiorno, PhD (Kathleen.delgiorno@vanderbilt.edu).

Materials availability

Pcdh20-/- mice were generated in this study and require a material transfer agreement (MTA). ESPIN antibody and Tmc1-mCherry mice are available from Dr. Bechara Kachar. PCDH20 antibody and Pcdh20-GFP plasmids are available from Dr. Qizhi Gong. All other materials are available from the lead contact upon request pending MTA.

Data and code availability

The POU2F3 ChIP-seq dataset generated for this study is available GEO GSE116510. Any information needed to reanalyze data from this study is available upon request from the lead contact.

ACKNOWLEDGEMENTS

The authors would like to thank Jakob von Moltke for supplying tuft cell EM images and Claire O'Leary for supplying gallbladder scRNA-seq data and for critical reading of the manuscript. KEA is supported by NIH NIDDK T32DK007673. YY and KSL are funded by R01DK103831 and U54CA274367. Salk Institute Core Facilities are supported, in part, by the NIH/NCI Cancer Center Support Grant (P30 014195), the Chapman Foundation, the Helmsley Charitable Trust, and the Waitt Foundation. ND is supported by the Rita Allen Foundation Scholars Award. SE is supported by the Owens Family Foundation. BK was supported by NIDCD-NIH-IRP funds Z01-DC000002. Electron microscopy was done in part by the Vanderbilt Cell Imaging Shared Resource supported by NIH Grants CA68485, DK20593, DK58404, DK59637, EY08126, 1S10OD034315, and 1R24OD037694. QG is supported by NIH R01 DC019769. U.M. is supported by a CZI Imaging Scientist Award from the Chan Zuckerberg Initiative DAF, NSF NeuroNex Award 2014862, the David F. And Margaret T. Grohne Family Foundation, the G. Harold & Leila Y. Mathers Foundation, NIDCD R01 DC021075, and the UCSD Goeddel Family Technology Sandbox. The DelGiorno laboratory was supported by the Vanderbilt Ingram Cancer Center Support Grant (NIH/NCI P30CA068485), the Vanderbilt Ingram Cancer Center SPORE in Gastrointestinal Cancer (NIH/NCI P50CA236733), the Vanderbilt Digestive Disease Research Center (NIH/NIDDK P30DK058404), an American Gastroenterological Association Research Scholar Award (AGA2021-13), NIH/NIGMS R35GM142709, The Department of Defense (DOD W81XWH2211121), The Sky Foundation, Inc (AWD00000079), the American Cancer Society (CAT-24-1374680-01-CAT), and Linda's Hope (Nashville, TN).

AUTHOR CONTRIBUTIONS

K.E.D and K.E.A. prepared the manuscript. K.E.D. conceptualized and supervised the study. K.E.A., contributed to the study design and was co-lead on experiments, imaging and data analysis. Y.Y., C-Y.C., L.R.A, S.W.N, B.J., W.H.A., J.L., V.S., and E.K. provided technical support. C-Y.C., L.R.A., S.W.N., N.D., E.K., and K.S.L, provided supporting roles for methodology. C.E.O., S.E., B.K., Q.G., G.M.W., and U.M., provided materials and helped with discussions.

DECLARATION OF INTERESTS

The authors declare no conflicts.

SUPPLEMENTAL INFORMATION

Document S1. Figures S1-S7 and Table S1

File S1. POU2F3 ChIP-seq

File S2. ChIP-seq_Tuft_Hair cell overlap

File S3. Human_Mouse_POU2F3 ChIP-seq comparison

File S4. Tuft_Hair cell overlap GO analysis

FIGURE LEGENDS

Figure 1. ChIP-seq identifies POU2F3 target genes in tuft cells. (**A**) POU2F3 and IgG control ChIP-seq signal. (**B**) Bar graph demonstrating enrichment of POU2F3 peaks in gene promoters. (**C**) Motif analysis identifying likely POU2F3 consensus binding sequences (**D**) Tracks showing POU2F3 binding sites in canonical tuft cell genes. (**E**) Venn diagram of POU2F3 ChIP-seq target genes and differentially expressed genes identified as either up- or down-regulated in duodenal tuft cells as compared to non-tuft epithelial cells by RNA-seq[11]. (**F**) Venn diagram of POU2F3 ChIP-seq target genes in either normal murine tuft cells or in a human cell line of a tuft-like variant of non-small cell lung cancer[42].(**G**) Genomic Regions Enrichment of Annotations (GREAT) analysis of POU2F3 ChIP-seq target genes. See also Figure S1-S2.

Figure 2. POU2F3 ChIP-seq reveals a cochlear hair cell transcriptomic signature. (**A**) Scanning electron microscopy of a thin tissue section of a small intestinal tuft cell, highlighting the microvillar structure. Scale bars, 1 μm. (**B**) Venn diagram of POU2F3 ChIP-seq target genes and a murine cochlear hair cell RNA-seq dataset generated in a study by Jean et al[27]. (**C**) Select genes from the 825 common to both datasets in (B). (**D**) Tracks showing POU2F3 binding sites in tuft cells for genes expressed in cochlear hair cells including known markers (*Espn*, *Clic5*, *Whrn*, *Tmc1*) and protocadherin 20 (*Pcdh20*). (**E**) Gene Ontology (GO) analysis of the 825 genes common to both the intestinal tuft cell POU2F3 ChIP-seq dataset and the hair cell RNA-seq dataset, highlighting structure-function pathways. See also Figures S3.

Figure 3. PCDH20 is a tuft cell-specific protocadherin in the gut epithelium. (**A**) Principal component analysis (PCA) comparing the transcriptomes of tuft cells from the murine small intestines, colon, gallbladder, thymus, and trachea, and non-tuft intestinal epithelial cells generated by the study from Nadjsombati et al[7]. (**B**) Expression of *Espn*, *Clic5*, and *Pcdh20* in the datasets in (A). (**C**) PCA comparing the transcriptomes of tuft cells from the normal murine duodenum, caerulein-induced chronic pancreatitis, or *Kras*^{G12D}-induced pancreatic neoplasia generated by studies from DelGiorno et al[11,29]. (**D**) Expression of *Espn*, *Clic5*, and *Pcdh20* in the datasets in (C). (**E**) Uniform manifold approximation and projection (UMAP) of murine gallbladder collected from either wild-type or *Pou2f3-/-* mice generated by a study from O'Leary

et al[10]. (**F**) UMAPs of *Espn*, *Clic5*, or *Pcdh20* expression in either wild-type or *Pou2f3-/-* gallbladders. Data are represented as mean +/- SD. See also Figure S4.

Figure 4. PCDH20 localizes to tuft cell microvilli. Co-Immunofluorescence (co-IF) staining of tuft cells in the murine small intestines or gallbladder for F-actin (phalloidin, white), DAPI (blue) and either (**A-B**) Espin or (**C-D**) PCDH20, scale bars 2 μm. Co-IF for TMC1 (magenta) and F-actin (phalloidin, green) in tuft cells in the (**E**) gallbladder or (**F**) small intestines. Scale bars, 5 μm. 2° only, secondary antibody staining only. See also Figures S5-6.

Figure 5. High resolution ultramicroscopy reveals intermicrovillar linkages in tuft cells. (**A**) SEM of the apical surface of the murine gallbladder, scale bar, 6 μm and (**B-C**) a tuft cell highlighting links between microvilli. Scale bars, 2 μm and 1 μm, respectively. (**D-E**) Transmission electron microscopy (TEM) of a gallbladder tuft cell highlighting links between tuft cell microvilli as well as between the tuft and a surrounding cell. Scale bars, 400 nm. White arrows, intermicrovillar tuft cell links. Black arrows, links between tuft and neighboring cell. Scanning electron microscopy (SEM) of (**F**) a normal intestinal villus at low magnification, scale bar, 3 μm, and (**G-H**) a tuft cell highlighting the apical microvilli, scale bars, 2 nm. (**I-J**) Freeze etch electron microscopy revealing extensive intermicrovillar linkages in intestinal tuft cells. Scale bars, 500 nm.

Figure 6. PCDH20 maintains tuft cell microvillar structure and rigidity. (**A**) Immunogold labeling of PCDH20 in a gallbladder tuft cell. Scale bar, 200 nm. (**B**) Co-IF for PCDH20 (green), phalloidin (red) and DAPI (blue) in tuft cells from both wild-type and PCDH20-/- small intestines. Scale bars, 5 μm. (**C**) SEM of a gallbladder tuft cell from a *Pcdh20+/+* mouse. Scale bar, 1 μm. (**D-E**) SEM of a gallbladder tuft cell from a *Pcdh20-/-* mouse highlighting impaired microvilli. Scale bars, 800 nm and 200 nm, respectively. Quantification of SEM images from *Pcdh20-/-* and control mouse for (**F**) extracellular, apical tuft cell size, (**G**) microvilli number per tuft cell, (**H**) microvilli angle, with illustration, scale bar 1 μm, (**I**) number of vesicles per tuft cells, (**J**) number of vesicles per microvilli, and (**K**) average vesicle size, with illustration, scale bar, 1 μm. Data are represented as mean +/- SD. See also Figures S7-8.

Figure 7. Model for PCDH20 in tuft cell intermicrovilliar linkages. Based on ChIP-seq, immunofluorescence, and EM studies, PCDH20 likely acts a structural component of intermicrovillar linkages in tuft cells. Whether PCDH20 interacts with CDHR5 and/or CDHR2 has yet to be determined. PCDH20 may function in all linkages or in a subset, excluded from CDHR5-CDHR2 interactions. Should PCDH20 function in a manner similar to tip links in hair cells, it would directly interact with TMC channels and tension would result in channel opening and cellular depolarization. Whirlin and Espin function in actin cytoskeleton assembly.

REFERENCES

1. Sato, A. (2007). Tuft cells. Anat Sci Int *82*, 187-199. 10.1111/j.1447-073X.2007.00188.x.
2. Luciano, L., and Reale, E. (1997). Presence of brush cells in the mouse gallbladder. Microsc Res Tech *38*, 598-608. 10.1002/(SICI)1097-0029(19970915)38:6<598::AID-JEMT4>3.0.CO;2-B.
3. Jarvi, O., and Keyrilainen, O. (1956). On the cellular structures of the epithelial invasions in the glandular stomach of mice caused by intramural application of 20-methylcholantren. Acta Pathol Microbiol Scand Suppl *39*, 72-73.
4. Gerbe, F., Sidot, E., Smyth, D.J., Ohmoto, M., Matsumoto, I., Dardalhon, V., Cesses, P., Garnier, L., Pouzolles, M., Brulin, B., et al. (2016). Intestinal epithelial tuft cells initiate type 2 mucosal immunity to helminth parasites. Nature *529*, 226-230. 10.1038/nature16527.
5. von Moltke, J., Ji, M., Liang, H.E., and Locksley, R.M. (2016). Tuft-cell-derived IL-25 regulates an intestinal ILC2-epithelial response circuit. Nature *529*, 221-225. 10.1038/nature16161.
6. Howitt, M.R., Lavoie, S., Michaud, M., Blum, A.M., Tran, S.V., Weinstock, J.V., Gallini, C.A., Redding, K., Margolskee, R.F., Osborne, L.C., et al. (2016). Tuft cells, taste-chemosensory cells, orchestrate parasite type 2 immunity in the gut. Science *351*, 1329-1333. 10.1126/science.aaf1648.
7. Nadjsombati, M.S., McGinty, J.W., Lyons-Cohen, M.R., Jaffe, J.B., DiPeso, L., Schneider, C., Miller, C.N., Pollack, J.L., Nagana Gowda, G.A., Fontana, M.F., et al. (2018). Detection of Succinate by Intestinal Tuft Cells Triggers a Type 2 Innate Immune Circuit. Immunity *49*, 33-41 e37. 10.1016/j.immuni.2018.06.016.
8. Ualiyeva, S., Hallen, N., Kanaoka, Y., Ledderose, C., Matsumoto, I., Junger, W.G., Barrett, N.A., and Bankova, L.G. (2020). Airway brush cells generate cysteinyl leukotrienes through the ATP sensor P2Y2. Sci Immunol *5*. 10.1126/sciimmunol.aax7224.
9. Keshavarz, M., Faraj Tabrizi, S., Ruppert, A.L., Pfeil, U., Schreiber, Y., Klein, J., Brandenburger, I., Lochnit, G., Bhushan, S., Perniss, A., et al. (2022). Cysteinyl leukotrienes and acetylcholine are biliary tuft cell cotransmitters. Sci Immunol *7*, eabf6734. 10.1126/sciimmunol.abf6734.
10. O'Leary, C.E., Sbierski-Kind, J., Kotas, M.E., Wagner, J.C., Liang, H.E., Schroeder, A.W., de Tenorio, J.C., von Moltke, J., Ricardo-Gonzalez, R.R., Eckalbar, W.L., et al. (2022). Bile acid-sensitive tuft cells regulate biliary neutrophil influx. Sci Immunol *7*, eabj1080. 10.1126/sciimmunol.abj1080.
11. DelGiorno, K.E., Chung, C.Y., Vavinskaya, V., Maurer, H.C., Novak, S.W., Lytle, N.K., Ma, Z., Giraddi, R.R., Wang, D., Fang, L., et al. (2020). Tuft Cells Inhibit Pancreatic Tumorigenesis in Mice by Producing Prostaglandin D(2). Gastroenterology *159*, 1866-1881 e1868. 10.1053/j.gastro.2020.07.037.
12. O'Leary, C.E., Ma, Z., Culpepper, T., Novak, S.W., and DelGiorno, K.E. (2022). New insights into tuft cell formation: Implications for structure-function relationships. Curr Opin Cell Biol *76*, 102082. 10.1016/j.ceb.2022.102082.
13. Yamashita, J., Ohmoto, M., Yamaguchi, T., Matsumoto, I., and Hirota, J. (2017). Skn-1a/Pou2f3 functions as a master regulator to generate Trpm5-expressing chemosensory cells in mice. PLoS One *12*, e0189340. 10.1371/journal.pone.0189340.
14. Matsumoto, I., Ohmoto, M., Narukawa, M., Yoshihara, Y., and Abe, K. (2011). Skn-1a (Pou2f3) specifies taste receptor cell lineage. Nat Neurosci *14*, 685-687. 10.1038/nn.2820.
15. Howitt, M.R., Cao, Y.G., Gologorsky, M.B., Li, J.A., Haber, A.L., Biton, M., Lang, J., Michaud, M., Regev, A., and Garrett, W.S. (2020). The Taste Receptor TAS1R3 Regulates Small Intestinal Tuft Cell Homeostasis. Immunohorizons *4*, 23-32. 10.4049/immunohorizons.1900099.
16. Kinnamon, S.C., and Finger, T.E. (2019). Recent advances in taste transduction and signaling. F1000Res *8*. 10.12688/f1000research.21099.1.
17. Feng, X., Fluchter, P., De Tenorio, J.C., and Schneider, C. (2024). Tuft cells in the intestine, immunity and beyond. Nat Rev Gastroenterol Hepatol *21*, 852-868. 10.1038/s41575-024-00978-1.
18. Caprara, G.A., and Peng, A.W. (2022). Mechanotransduction in mammalian sensory hair cells. Mol Cell Neurosci *120*, 103706. 10.1016/j.mcn.2022.103706.
19. Cunningham, C.L., and Muller, U. (2019). Molecular Structure of the Hair Cell Mechanoelectrical Transduction Complex. Cold Spring Harb Perspect Med *9*. 10.1101/cshperspect.a033167.
20. Schmidl, C., Rendeiro, A.F., Sheffield, N.C., and Bock, C. (2015). ChIPmentation: fast, robust, low-input ChIP-seq for histones and transcription factors. Nat Methods *12*, 963-965. 10.1038/nmeth.3542.

21. Chung, C.Y., Sun, Z., Mullokandov, G., Bosch, A., Qadeer, Z.A., Cihan, E., Rapp, Z., Parsons, R., Aguirre-Ghiso, J.A., Farias, E.F., et al. (2016). Cbx8 Acts Non-canonically with Wdr5 to Promote Mammary Tumorigenesis. Cell Rep *16*, 472-486. 10.1016/j.celrep.2016.06.002.
22. Langmead, B., Trapnell, C., Pop, M., and Salzberg, S.L. (2009). Ultrafast and memory-efficient alignment of short DNA sequences to the human genome. Genome Biol *10*, R25. 10.1186/gb-2009-10-3-r25.
23. Zhang, Y., Liu, T., Meyer, C.A., Eeckhoute, J., Johnson, D.S., Bernstein, B.E., Nusbaum, C., Myers, R.M., Brown, M., Li, W., and Liu, X.S. (2008). Model-based analysis of ChIP-Seq (MACS). Genome Biol *9*, R137. 10.1186/gb-2008-9-9-r137.
24. Ramirez, F., Dundar, F., Diehl, S., Gruning, B.A., and Manke, T. (2014). deepTools: a flexible platform for exploring deep-sequencing data. Nucleic acids research *42*, W187-191. 10.1093/nar/gku365.
25. McLean, C.Y., Bristor, D., Hiller, M., Clarke, S.L., Schaar, B.T., Lowe, C.B., Wenger, A.M., and Bejerano, G. (2010). GREAT improves functional interpretation of cis-regulatory regions. Nature biotechnology *28*, 495-501. 10.1038/nbt.1630.
26. Heinz, S., Benner, C., Spann, N., Bertolino, E., Lin, Y.C., Laslo, P., Cheng, J.X., Murre, C., Singh, H., and Glass, C.K. (2010). Simple combinations of lineage-determining transcription factors prime cis-regulatory elements required for macrophage and B cell identities. Molecular cell *38*, 576-589. 10.1016/j.molcel.2010.05.004.
27. Jean, P., Wong Jun Tai, F., Singh-Estivalet, A., Lelli, A., Scandola, C., Megharba, S., Schmutz, S., Roux, S., Mechaussier, S., Sudres, M., et al. (2023). Single-cell transcriptomic profiling of the mouse cochlea: An atlas for targeted therapies. Proc Natl Acad Sci U S A *120*, e2221744120. 10.1073/pnas.2221744120.
28. Hao, Y., Stuart, T., Kowalski, M.H., Choudhary, S., Hoffman, P., Hartman, A., Srivastava, A., Molla, G., Madad, S., Fernandez-Granda, C., and Satija, R. (2024). Dictionary learning for integrative, multimodal and scalable single-cell analysis. Nat Biotechnol *42*, 293-304. 10.1038/s41587-023-01767-y.
29. DelGiorno, K.E., Naeem, R.F., Fang, L., Chung, C.Y., Ramos, C., Luhtala, N., O'Connor, C., Hunter, T., Manor, U., and Wahl, G.M. (2020). Tuft Cell Formation Reflects Epithelial Plasticity in Pancreatic Injury: Implications for Modeling Human Pancreatitis. Front Physiol *11*, 88. 10.3389/fphys.2020.00088.
30. Lee, W., Cheng, T.W., and Gong, Q. (2008). Olfactory sensory neuron-specific and sexually dimorphic expression of protocadherin 20. J Comp Neurol *507*, 1076-1086. 10.1002/cne.21569.
31. Schindelin, J., Arganda-Carreras, I., Frise, E., Kaynig, V., Longair, M., Pietzsch, T., Preibisch, S., Rueden, C., Saalfeld, S., Schmid, B., et al. (2012). Fiji: an open-source platform for biological-image analysis. Nat Methods *9*, 676-682. 10.1038/nmeth.2019.
32. Horstmann, H., Korber, C., Satzler, K., Aydin, D., and Kuner, T. (2012). Serial section scanning electron microscopy (S3EM) on silicon wafers for ultra-structural volume imaging of cells and tissues. PLoS One *7*, e35172. 10.1371/journal.pone.0035172.
33. Seligman, A.M., Wasserkrug, H.L., and Hanker, J.S. (1966). A new staining method (OTO) for enhancing contrast of lipid--containing membranes and droplets in osmium tetroxide--fixed tissue with osmiophilic thiocarbohydrazide(TCH). J Cell Biol *30*, 424-432. 10.1083/jcb.30.2.424.
34. Walton, J. (1979). Lead aspartate, an en bloc contrast stain particularly useful for ultrastructural enzymology. J Histochem Cytochem *27*, 1337-1342. 10.1177/27.10.512319.
35. Harris, K.M., Perry, E., Bourne, J., Feinberg, M., Ostroff, L., and Hurlburt, J. (2006). Uniform serial sectioning for transmission electron microscopy. J Neurosci *26*, 12101-12103. 10.1523/JNEUROSCI.3994-06.2006.
36. Krey, J.F., Krystofiak, E.S., Dumont, R.A., Vijayakumar, S., Choi, D., Rivero, F., Kachar, B., Jones, S.M., and Barr-Gillespie, P.G. (2016). Plastin 1 widens stereocilia by transforming actin filament packing from hexagonal to liquid. J Cell Biol *215*, 467-482. 10.1083/jcb.201606036.
37. Ohmoto, M., Yamaguchi, T., Yamashita, J., Bachmanov, A.A., Hirota, J., and Matsumoto, I. (2013). Pou2f3/Skn-1a is necessary for the generation or differentiation of solitary chemosensory cells in the anterior nasal cavity. Biosci Biotechnol Biochem *77*, 2154-2156. 10.1271/bbb.130454.
38. Yamaguchi, T., Yamashita, J., Ohmoto, M., Aoude, I., Ogura, T., Luo, W., Bachmanov, A.A., Lin, W., Matsumoto, I., and Hirota, J. (2014). Skn-1a/Pou2f3 is required for the generation of Trpm5-expressing microvillous cells in the mouse main olfactory epithelium. BMC Neurosci *15*, 13. 10.1186/1471-2202-15-13.

39. Lena, A.M., Cipollone, R., Amelio, I., Catani, M.V., Ramadan, S., Browne, G., Melino, G., and Candi, E. (2010). Skn-1a/Oct-11 and DeltaNp63alpha exert antagonizing effects on human keratin expression. Biochem Biophys Res Commun *401*, 568-573. 10.1016/j.bbrc.2010.09.102.
40. Lammers, S., Barrera, V., Brennecke, P., Miller, C., Yoon, J., Balolong, J., Anderson, M.S., Ho Sui, S., Steinmetz, L.M., von Andrian, U.H., and Rattay, K. (2023). Ehf and Fezf2 regulate late medullary thymic epithelial cell and thymic tuft cell development. Front Immunol *14*, 1277365. 10.3389/fimmu.2023.1277365.
41. Gerbe, F., van Es, J.H., Makrini, L., Brulin, B., Mellitzer, G., Robine, S., Romagnolo, B., Shroyer, N.F., Bourgaux, J.F., Pignodel, C., et al. (2011). Distinct ATOH1 and Neurog3 requirements define tuft cells as a new secretory cell type in the intestinal epithelium. J Cell Biol *192*, 767-780. 10.1083/jcb.201010127.
42. Wu, X.S., He, X.Y., Ipsaro, J.J., Huang, Y.H., Preall, J.B., Ng, D., Shue, Y.T., Sage, J., Egeblad, M., Joshua-Tor, L., and Vakoc, C.R. (2022). OCA-T1 and OCA-T2 are coactivators of POU2F3 in the tuft cell lineage. Nature *607*, 169-175. 10.1038/s41586-022-04842-7.
43. Ruppert, A.L., Keshavarz, M., Winterberg, S., Oberwinkler, J., Kummer, W., and Schutz, B. (2020). Advillin is a tuft cell marker in the mouse alimentary tract. J Mol Histol *51*, 421-435. 10.1007/s10735-020-09893-6.
44. Stubler, R., Dooley, S.A., Edens, R., Nicholson, M.R., and Engevik, A.C. (2024). Intestinal Tuft Cells Are Enriched With Protocadherins. J Histochem Cytochem *72*, 611-622. 10.1369/00221554241287267.
45. Kasper, M., Hofer, D., Woodcock-Mitchell, J., Migheli, A., Attanasio, A., Rudolf, T., Muller, M., and Drenckhahn, D. (1994). Colocalization of cytokeratin 18 and villin in type III alveolar cells (brush cells) of the rat lung. Histochemistry *101*, 57-62. 10.1007/BF00315832.
46. Lorente-Canovas, B., Eckrich, S., Lewis, M.A., Johnson, S.L., Marcotti, W., and Steel, K.P. (2022). Grxcr1 regulates hair bundle morphogenesis and is required for normal mechanoelectrical transduction in mouse cochlear hair cells. PLoS One *17*, e0261530. 10.1371/journal.pone.0261530.
47. Kitano, T., Kitajiri, S.I., Nishio, S.Y., and Usami, S.I. (2019). Detailed Clinical Features of Deafness Caused by a Claudin-14 Variant. Int J Mol Sci *20*. 10.3390/ijms20184579.
48. Friedman, T.B., Sellers, J.R., and Avraham, K.B. (1999). Unconventional myosins and the genetics of hearing loss. Am J Med Genet *89*, 147-157. 10.1002/(sici)1096-8628(19990924)89:3<147::aid-ajmg5>3.0.co;2-6.
49. Sekerkova, G., Zheng, L., Loomis, P.A., Changyaleket, B., Whitlon, D.S., Mugnaini, E., and Bartles, J.R. (2004). Espins are multifunctional actin cytoskeletal regulatory proteins in the microvilli of chemosensory and mechanosensory cells. J Neurosci *24*, 5445-5456. 10.1523/JNEUROSCI.1279-04.2004.
50. Zheng, L., Sekerkova, G., Vranich, K., Tilney, L.G., Mugnaini, E., and Bartles, J.R. (2000). The deaf jerker mouse has a mutation in the gene encoding the espin actin-bundling proteins of hair cell stereocilia and lacks espins. Cell *102*, 377-385. 10.1016/s0092-8674(00)00042-8.
51. Seco, C.Z., Oonk, A.M., Dominguez-Ruiz, M., Draaisma, J.M., Gandia, M., Oostrik, J., Neveling, K., Kunst, H.P., Hoefsloot, L.H., del Castillo, I., et al. (2015). Progressive hearing loss and vestibular dysfunction caused by a homozygous nonsense mutation in CLIC5. Eur J Hum Genet *23*, 189-194. 10.1038/ejhg.2014.83.
52. Singh, H., Cousin, M.A., and Ashley, R.H. (2007). Functional reconstitution of mammalian 'chloride intracellular channels' CLIC1, CLIC4 and CLIC5 reveals differential regulation by cytoskeletal actin. FEBS J *274*, 6306-6316. 10.1111/j.1742-4658.2007.06145.x.
53. Gagnon, L.H., Longo-Guess, C.M., Berryman, M., Shin, J.B., Saylor, K.W., Yu, H., Gillespie, P.G., and Johnson, K.R. (2006). The chloride intracellular channel protein CLIC5 is expressed at high levels in hair cell stereocilia and is essential for normal inner ear function. J Neurosci *26*, 10188-10198. 10.1523/JNEUROSCI.2166-06.2006.
54. Mburu, P., Mustapha, M., Varela, A., Weil, D., El-Amraoui, A., Holme, R.H., Rump, A., Hardisty, R.E., Blanchard, S., Coimbra, R.S., et al. (2003). Defects in whirlin, a PDZ domain molecule involved in stereocilia elongation, cause deafness in the whirler mouse and families with DFNB31. Nat Genet *34*, 421-428. 10.1038/ng1208.
55. Wu, S., Lin, L., Hu, Q., Yao, X., Wang, H., Liu, S., Liu, Q., Xi, Y., Lin, Y., Gong, J., et al. (2025). Mechano-electrical transduction components TMC1-CIB2 undergo a Ca(2+)-induced conformational change linked to hearing loss. Dev Cell. 10.1016/j.devcel.2025.01.004.
56. Vuckovic, D., Dawson, S., Scheffer, D.I., Rantanen, T., Morgan, A., Di Stazio, M., Vozzi, D., Nutile, T., Concas, M.P., Biino, G., et al. (2015). Genome-wide association analysis on normal hearing

function identifies PCDH20 and SLC28A3 as candidates for hearing function and loss. Hum Mol Genet *24*, 5655-5664. 10.1093/hmg/ddv279.
57. Delgiorno, K.E., Hall, J.C., Takeuchi, K.K., Pan, F.C., Halbrook, C.J., Washington, M.K., Olive, K.P., Spence, J.R., Sipos, B., Wright, C.V., et al. (2014). Identification and manipulation of biliary metaplasia in pancreatic tumors. Gastroenterology *146*, 233-244 e235. 10.1053/j.gastro.2013.08.053.
58. Silverman, J.B., Vega, P.N., Tyska, M.J., and Lau, K.S. (2024). Intestinal Tuft Cells: Morphology, Function, and Implications for Human Health. Annu Rev Physiol *86*, 479-504. 10.1146/annurev-physiol-042022-030310.
59. Ebrahim, S., Ballesteros, A., Zheng, W.S., Mukherjee, S., Hu, G., Weng, W.H., Montgomery, J.S., Agyemang, Y., Cui, R., Sun, W., et al. (2024). Transmembrane channel-like 4 and 5 proteins at microvillar tips are potential ion channels and lipid scramblases. bioRxiv. 10.1101/2024.08.22.609173.
60. Ma, Z., Lytle, N.K., Chen, B., Jyotsana, N., Novak, S.W., Cho, C.J., Caplan, L., Ben-Levy, O., Neininger, A.C., Burnette, D.T., et al. (2022). Single-Cell Transcriptomics Reveals a Conserved Metaplasia Program in Pancreatic Injury. Gastroenterology *162*, 604-620 e620. 10.1053/j.gastro.2021.10.027.
61. Gracz, A.D., Samsa, L.A., Fordham, M.J., Trotier, D.C., Zwarycz, B., Lo, Y.H., Bao, K., Starmer, J., Raab, J.R., Shroyer, N.F., et al. (2018). Sox4 Promotes Atoh1-Independent Intestinal Secretory Differentiation Toward Tuft and Enteroendocrine Fates. Gastroenterology *155*, 1508-1523 e1510. 10.1053/j.gastro.2018.07.023.
62. Baldan, J., Camacho-Roda, J., Ballester, M., Hoj, K., Kurilla, A., Maurer, H.C., Arcila-Barrera, S., Lin, X., Pan, Z., Castro, J.L., et al. (2024). Resolution of Acinar Dedifferentiation Regulates Tissue Remodeling in Pancreatic Injury and Cancer Initiation. Gastroenterology *167*, 718-732 e718. 10.1053/j.gastro.2024.04.031.
63. Salas-Escabillas, D.J., Hoffman, M.T., Brender, S.M., Moore, J.S., Wen, H.J., Benitz, S., Davis, E.T., Long, D., Wombwell, A.M., Chianis, E.R.D., et al. (2024). Tuft cells transdifferentiate to neural-like progenitor cells in the progression of pancreatic cancer. Dev Cell. 10.1016/j.devcel.2024.12.003.
64. Caplan, L.R., Vavinskaya, V., Gelikman, D.G., Jyotsana, N., Trinh, V.Q., Olive, K.P., Tan, M.C.B., and DelGiorno, K.E. (2022). Enteroendocrine Cell Formation Is an Early Event in Pancreatic Tumorigenesis. Front Physiol *13*, 865452. 10.3389/fphys.2022.865452.

A

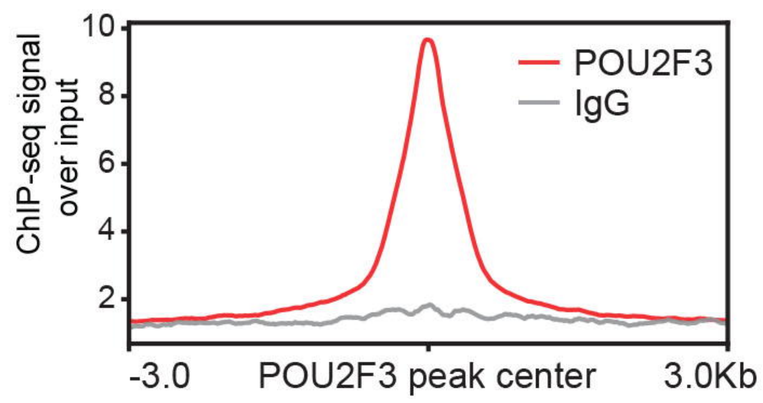

B

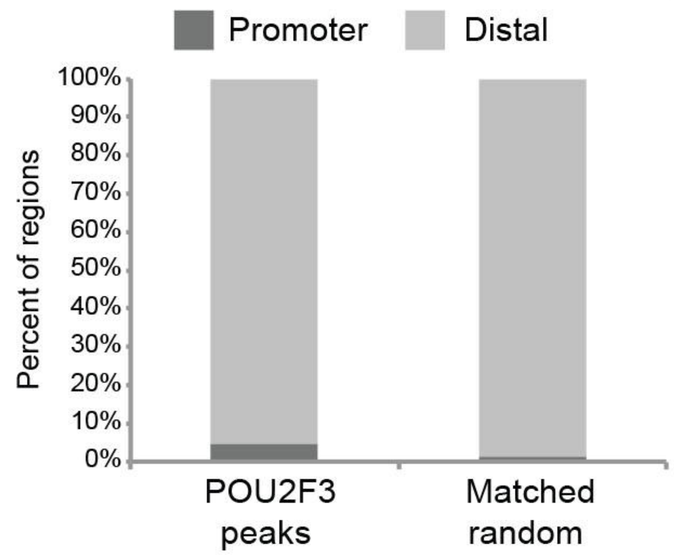

C

Rank	De novo motif	Best match	p-value
1		POU	$1x10^{-945}$
2		EHF	$1x10^{-39}$
3		RUNX	$1x10^{-36}$
4		SOX	$1x10^{-24}$

D

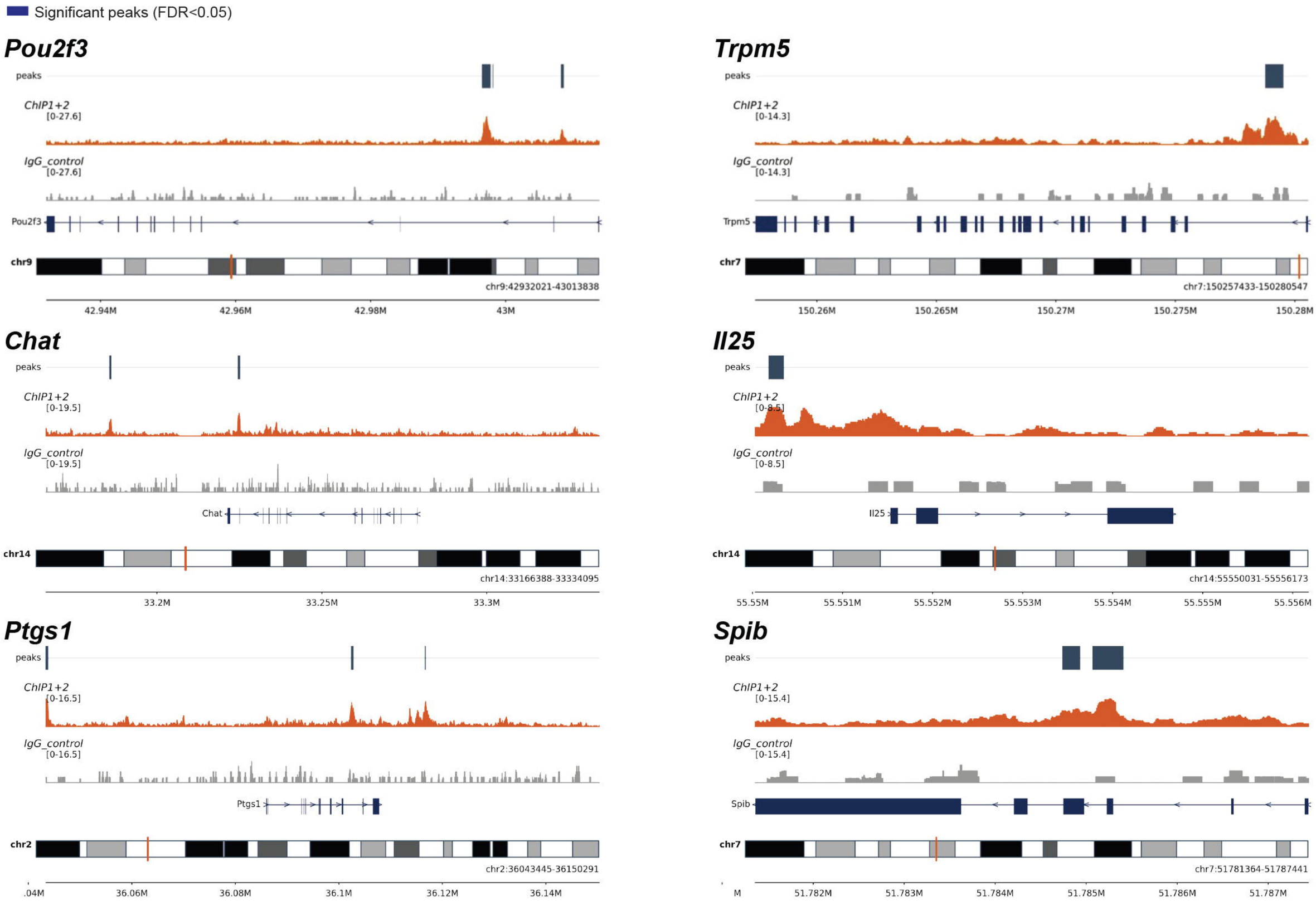

E

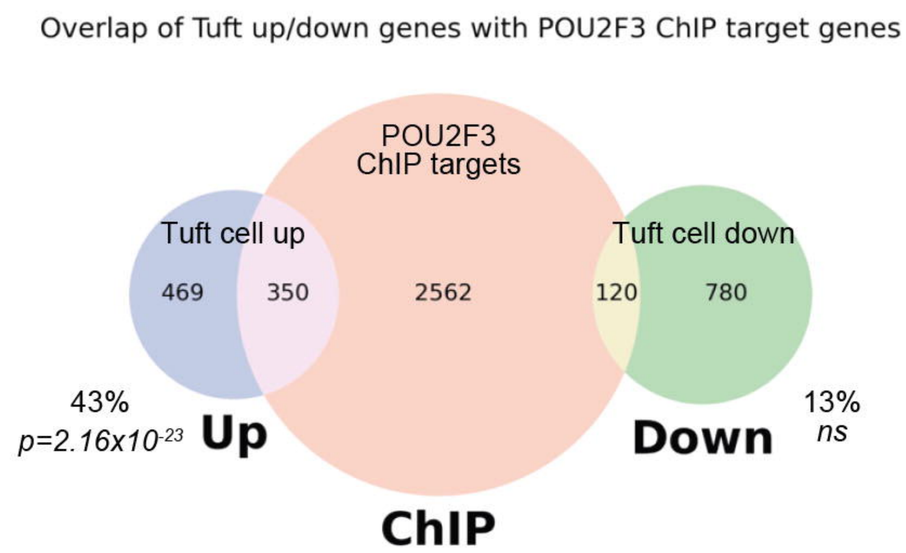

F

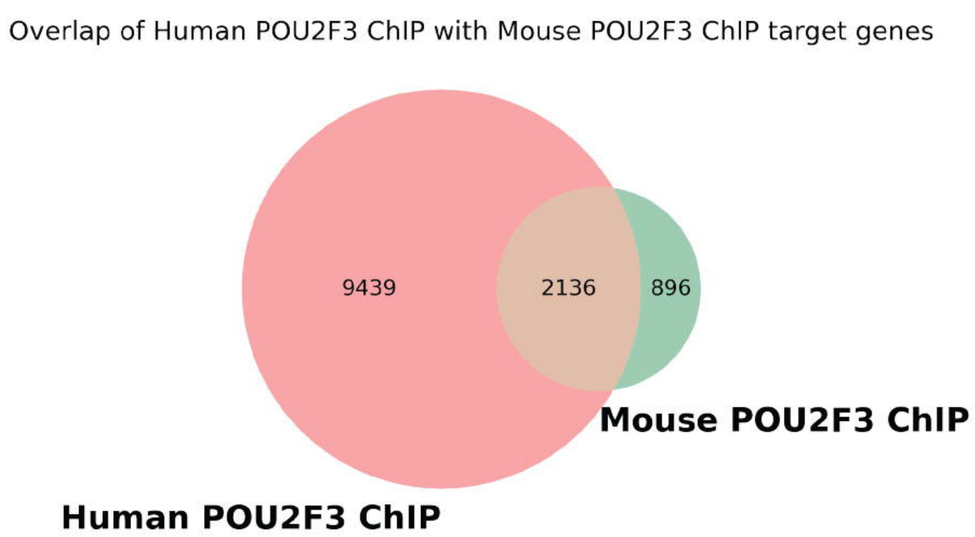

G

GO Biological Process	P-value
Membrane lipid metabolic process	$2.7x10^{-9}$
Regulation of toll-like receptor signaling pathway	$3.9x10^{-9}$
Cellular response to lipopolysaccharide	$3.6x10^{-8}$
Cellular response to molecule of bacterial origin	$1.3x10^{-7}$
Cellular response to biotic stimulus	$1.6x10^{-7}$
BioCyc Pathway	**P-value**
Biosynthesis of prostaglandins	$6.4x10^{-7}$
Fatty acid alpha-oxidation	$1.7x10^{-5}$
Ethanol degradation II (cytosol)	$1.7x10^{-5}$
Phenylalanine degradation III	$6.1x10^{-5}$
PANTHER Pathway	**P-value**
B cell activation	$1.2x10^{-8}$
T cell activation	$5.6x10^{-7}$
MSigDB Pathway	**P-value**
Genes involved in DARPP-32 events	$2.5x10^{-16}$
B cell receptor signaling pathway	$2.8x10^{-13}$
Fc gamma R-mediated phagocytosis	$1.4x10^{-12}$
VEGF signaling pathway	$1.3x10^{-11}$
Members of the BCR signaling pathway	$3.2x10^{-9}$

A

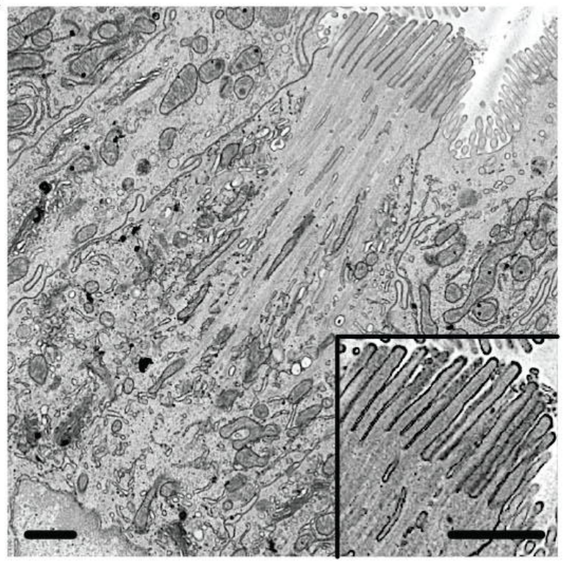

B

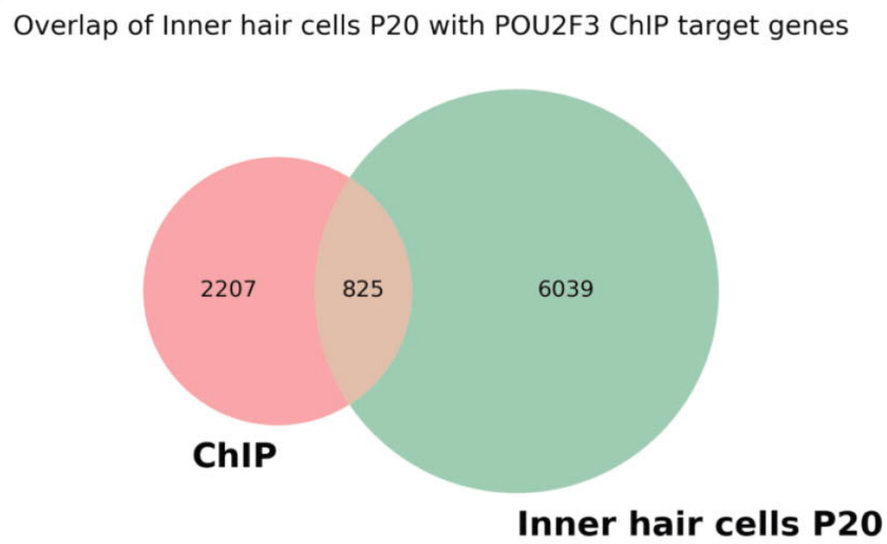

C

Espn	Cldn14	Eps8	Hspa2	Rab11a
Pcdh20	Mast2	Ahi1	Fam92a	Whrn
Tmc1	Plekha7	Vash2	Anxa4	Acsl1
Ccdc68	Myo6	Pmc1	Atp2b1	Pcbp1
Grxcr1	Aig1	Pebp1	Pgm1	Myo1e
Clic5	Rab39b	Prkar2a	Ppp1cb	Pitpnb
Cdh23	Twf1	Acot7	Mdh1	Tcf4
Atoh1	Rala	Vamp2	Dpysl2	Pcdh1

D

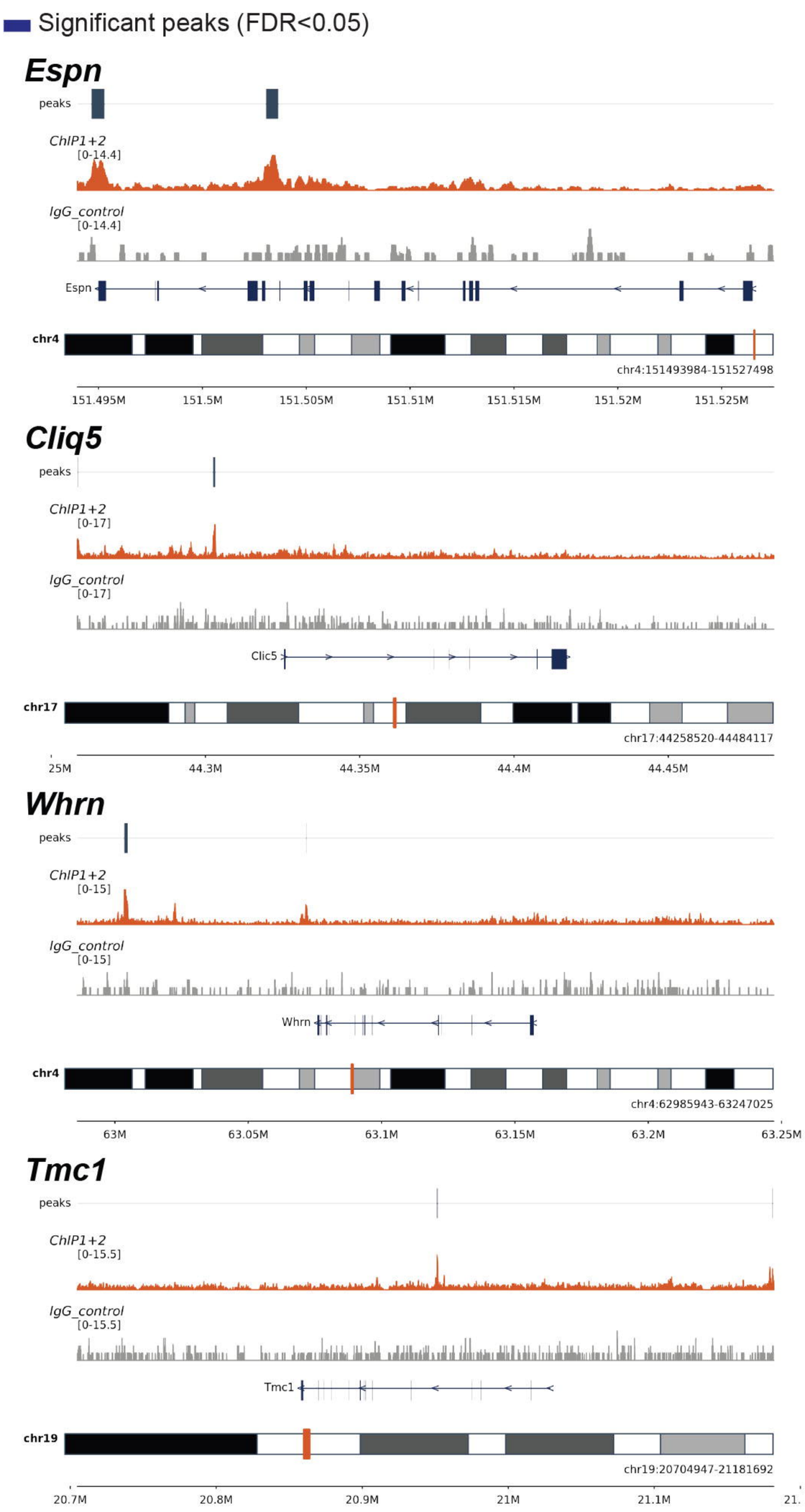

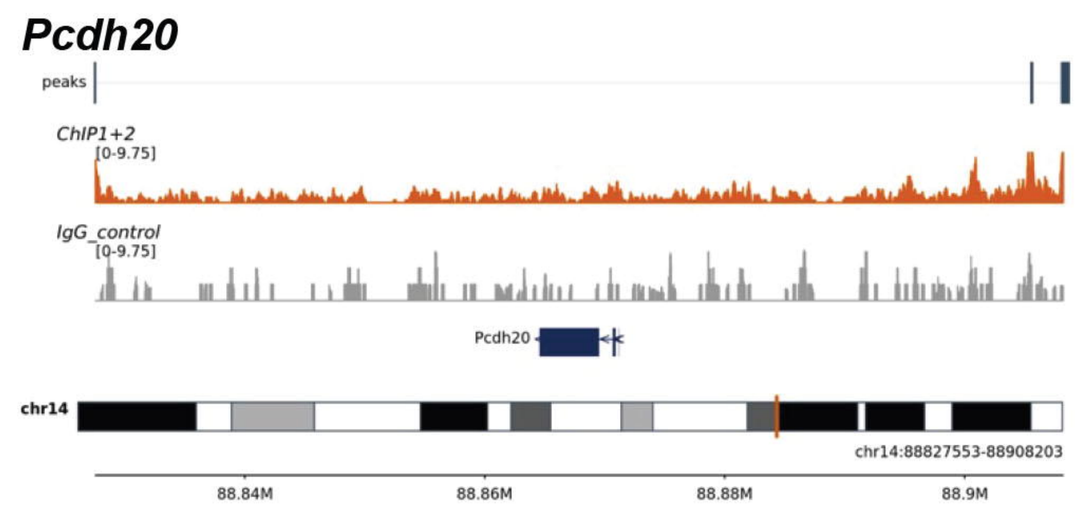

E

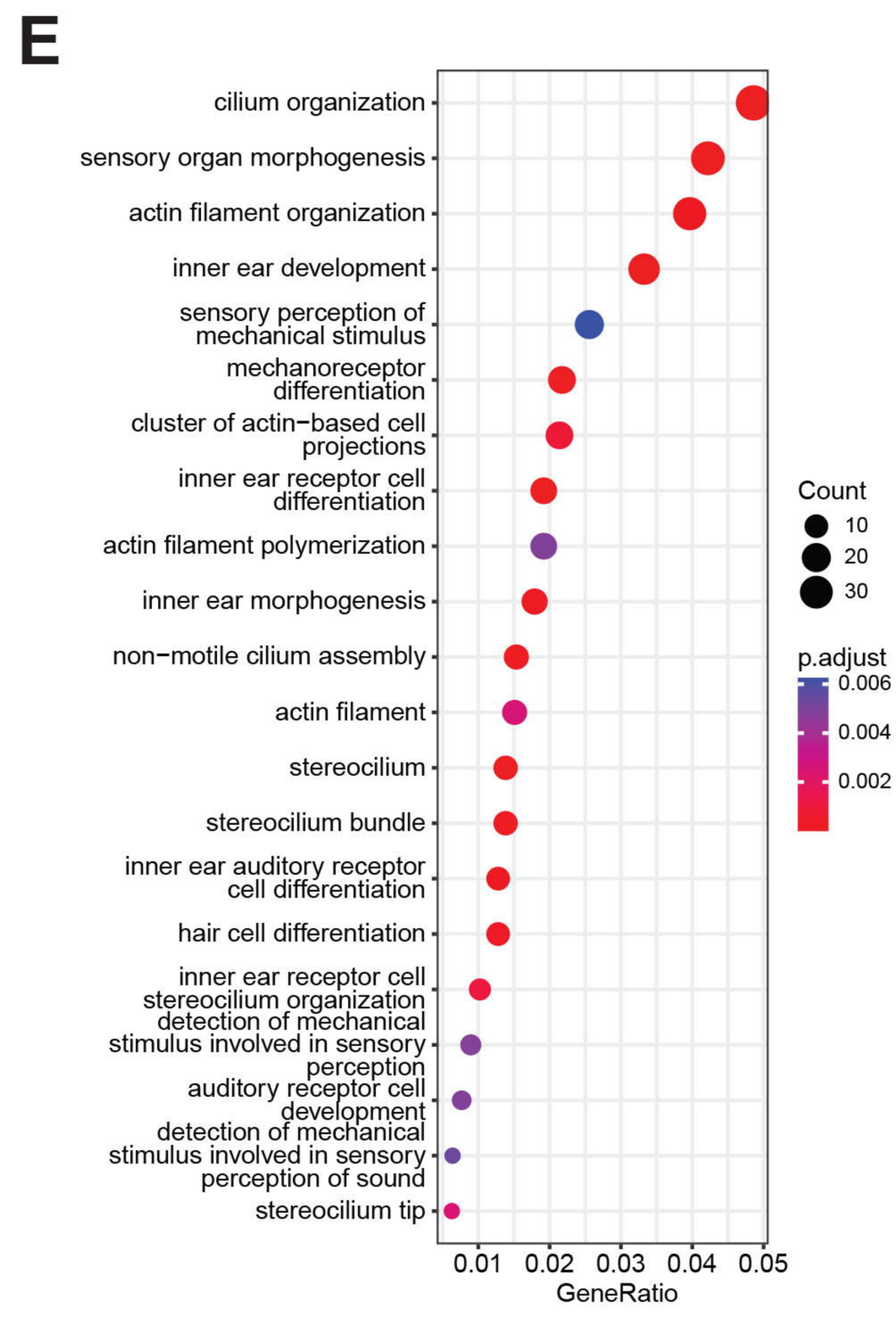

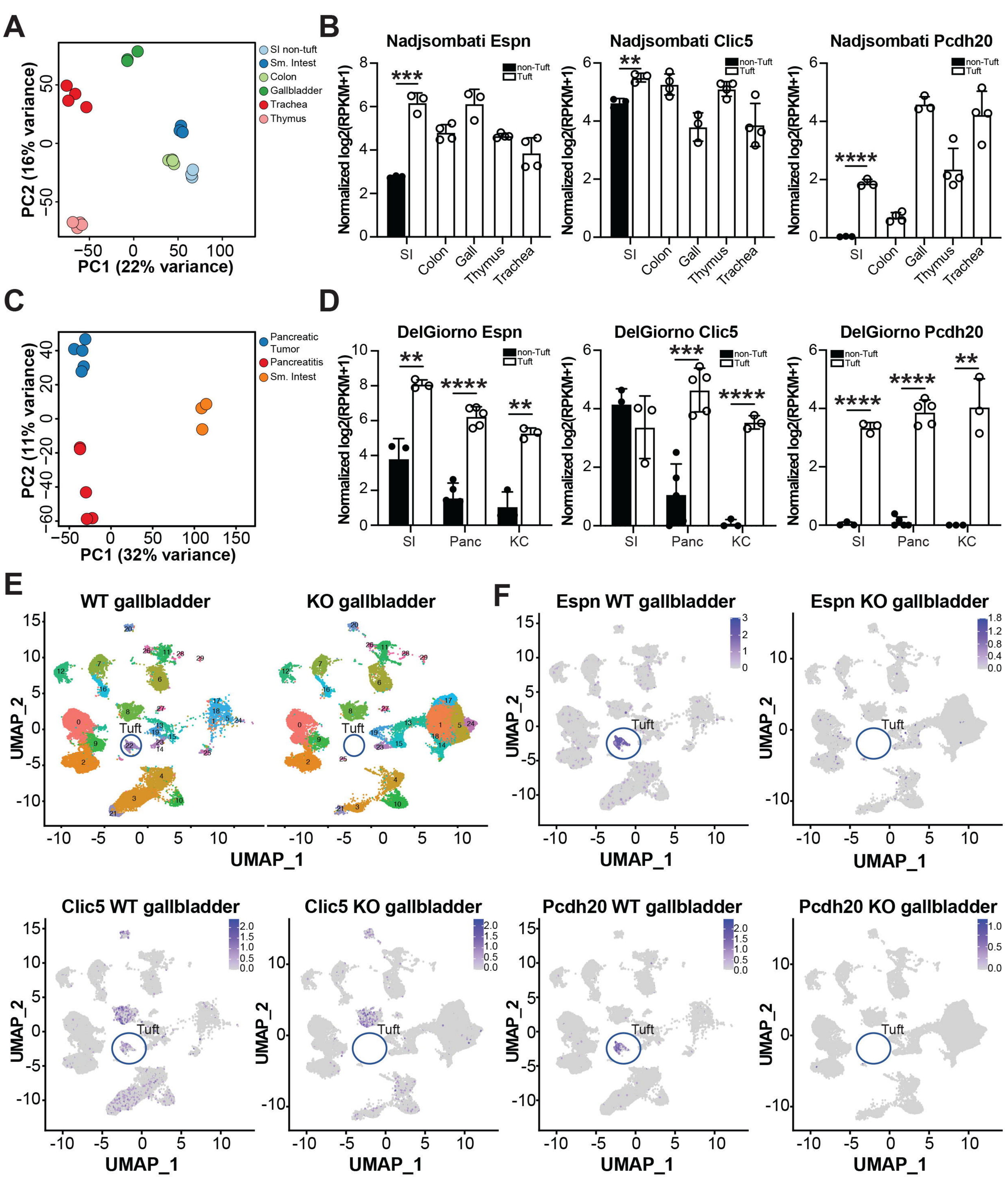
A
SI non-tuft
Sm. Intest
Colon
Gallbladder
Trachea
Thymus
PC2 (16% variance)
PC1 (22% variance)
B
Nadjsombati Espn
Nadjsombati Clic5
Nadjsombati Pcdh20
non-Tuft
Tuft
Normalized log2(RPKM+1)
SI
Colon
Gall
Thymus
Trachea
C
Pancreatic Tumor
Pancreatitis
Sm. Intest
PC2 (11% variance)
PC1 (32% variance)
D
DelGiorno Espn
DelGiorno Clic5
DelGiorno Pcdh20
SI
Panc
KC
E
WT gallbladder
KO gallbladder
Tuft
UMAP_1
UMAP_2
F
Espn WT gallbladder
Espn KO gallbladder
Clic5 WT gallbladder
Clic5 KO gallbladder
Pcdh20 WT gallbladder
Pcdh20 KO gallbladder

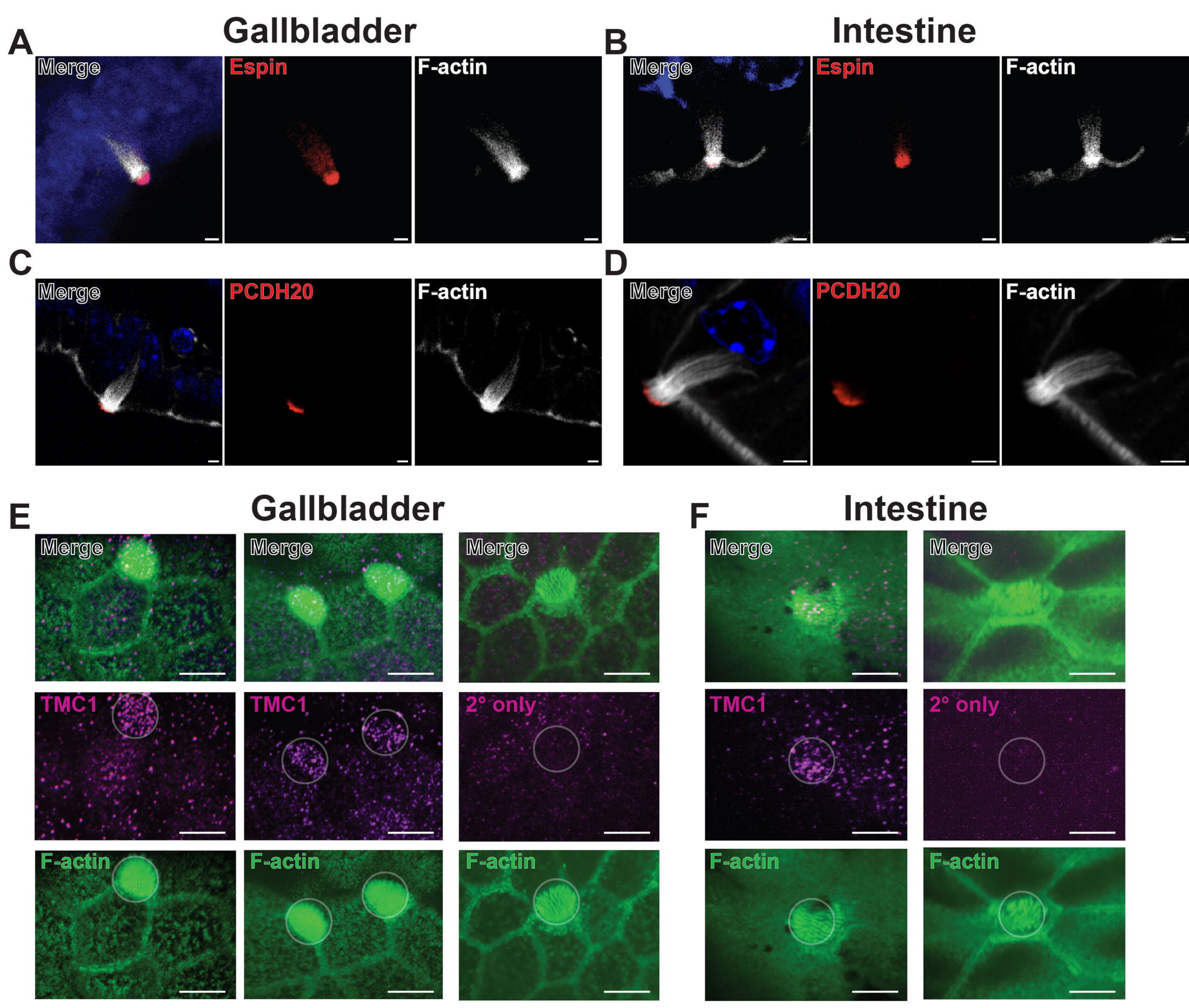
A
Gallbladder
Merge
Espin
F-actin
B
Intestine
Merge
Espin
F-actin
C
Merge
PCDH20
F-actin
D
Merge
PCDH20
F-actin
E
Gallbladder
Merge
Merge
Merge
TMC1
TMC1
2° only
F-actin
F-actin
F-actin
F
Intestine
Merge
Merge
TMC1
2° only
F-actin
F-actin

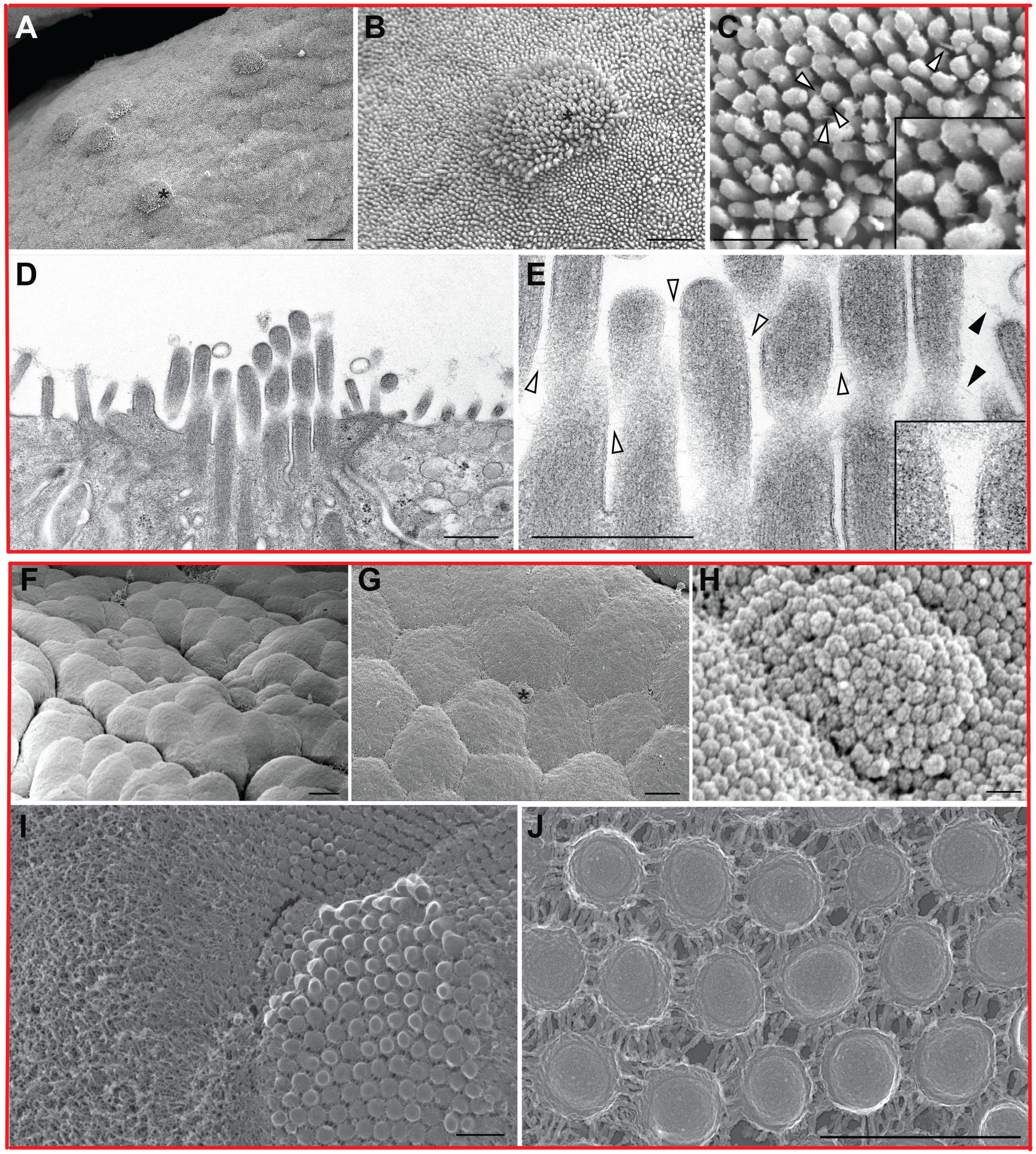
A
B
C
D
E
F
G
H
I
J

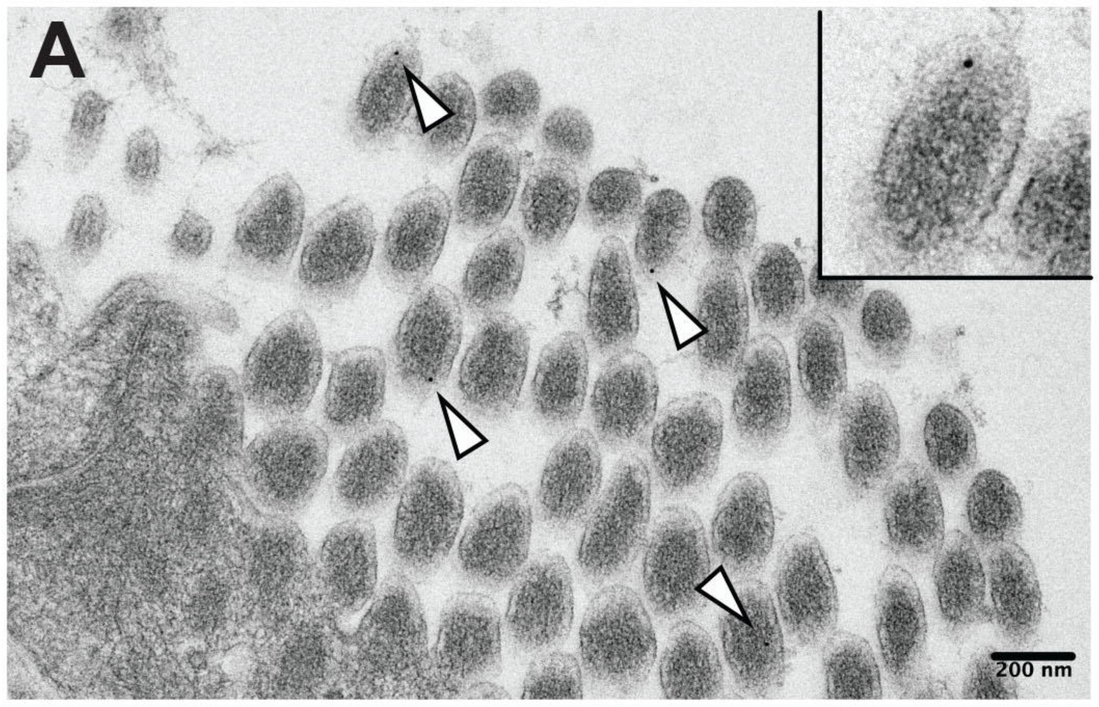
A
200 nm

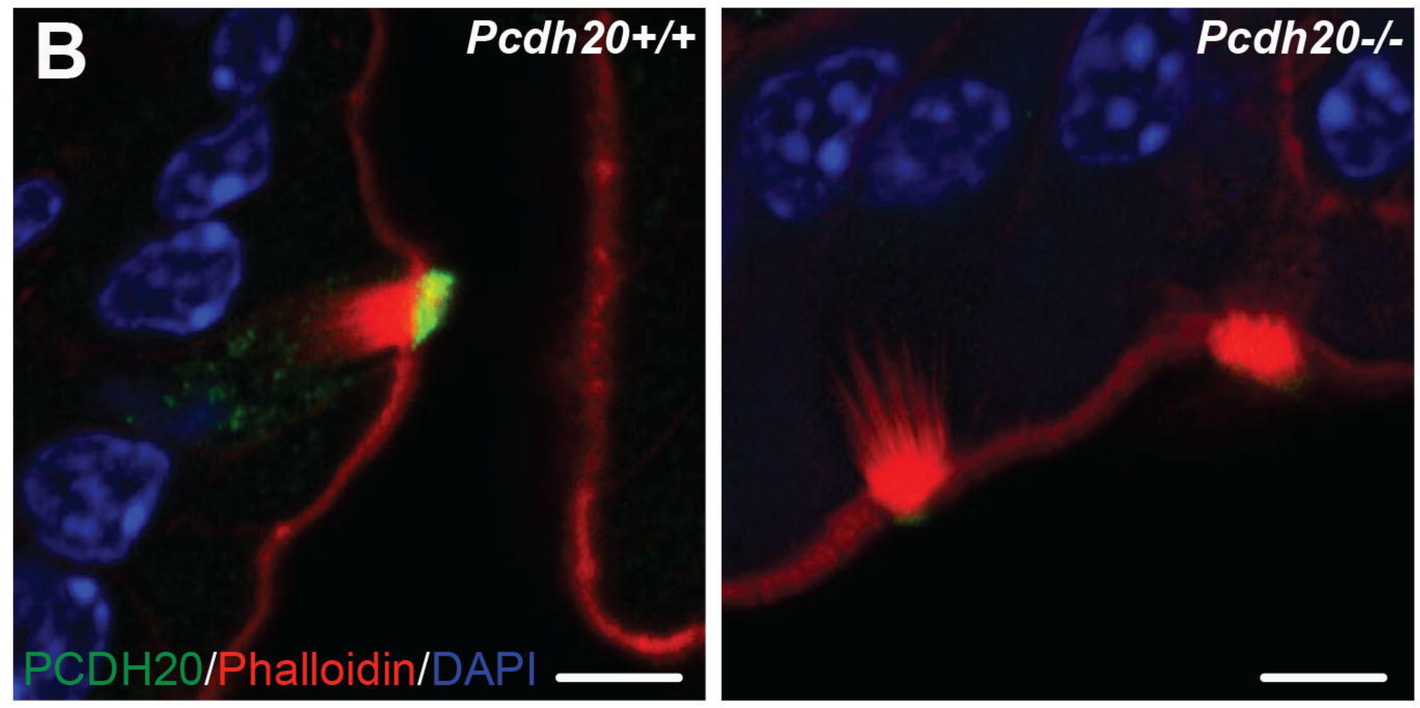
B
Pcdh20+/+
Pcdh20-/-
PCDH20/Phalloidin/DAPI

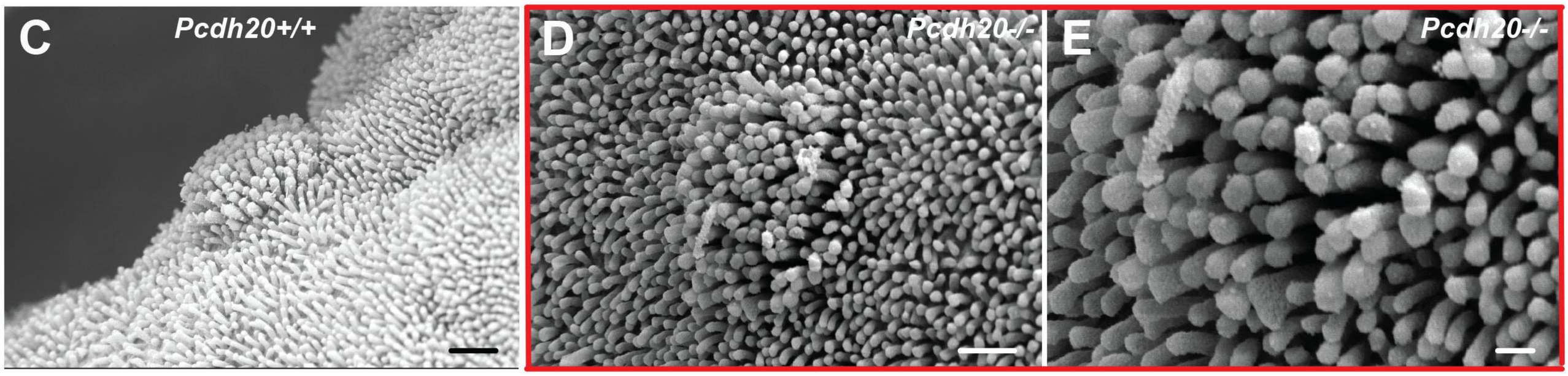
C
Pcdh20+/+
D
Pcdh20-/-
E
Pcdh20-/-

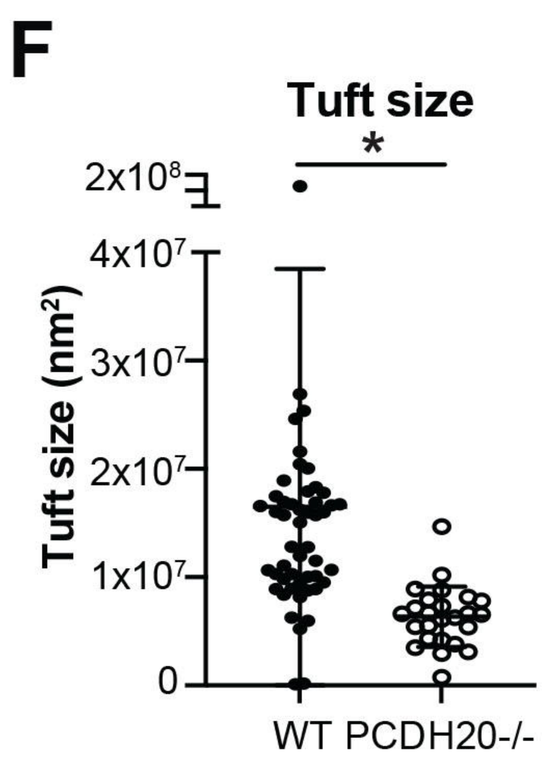
F
Tuft size
*
Tuft size (nm²)
2x10⁸
4x10⁷
3x10⁷
2x10⁷
1x10⁷
0
WT
PCDH20-/-

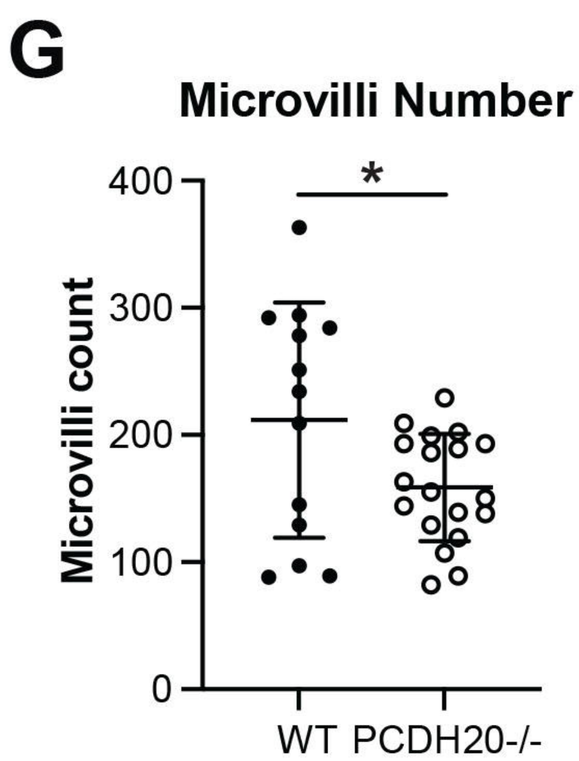
G
Microvilli Number
*
Microvilli count
400
300
200
100
0
WT
PCDH20-/-

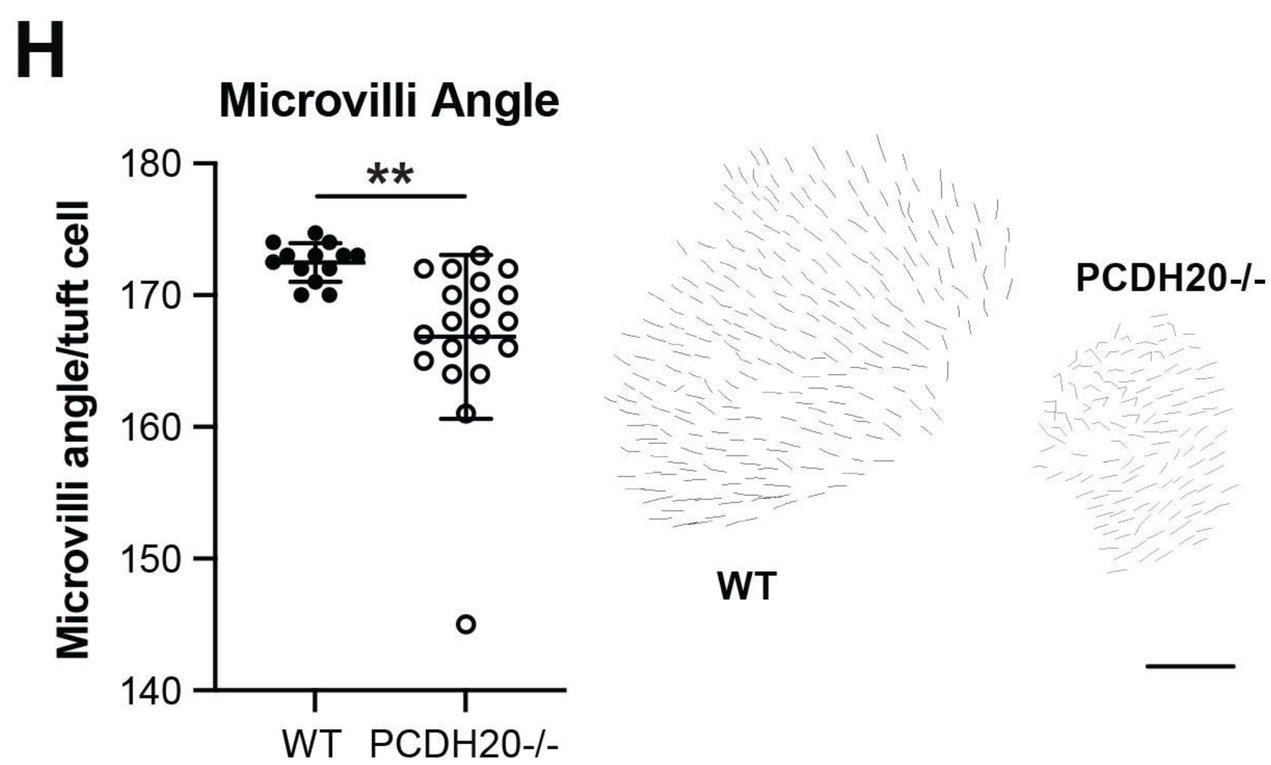
H
Microvilli Angle
**
Microvilli angle/tuft cell
180
170
160
150
140
WT
PCDH20-/-
PCDH20-/-
WT

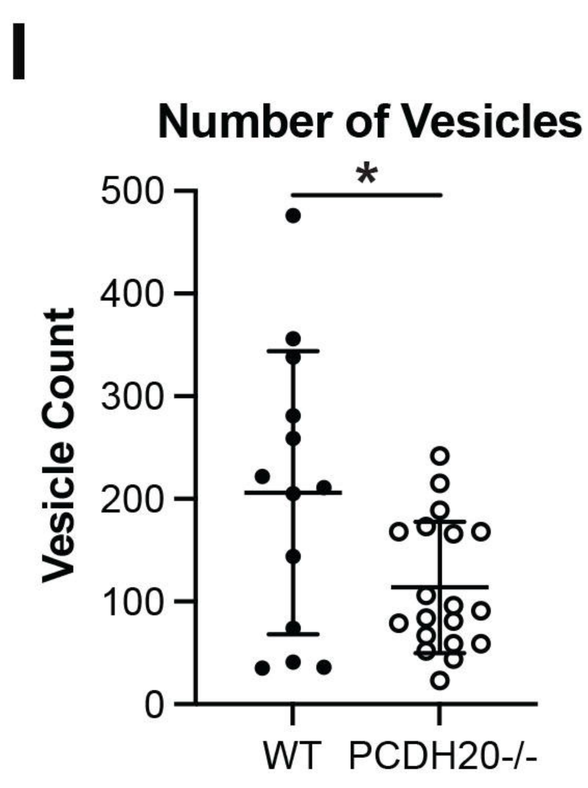
I
Number of Vesicles
*
Vesicle Count
500
400
300
200
100
0
WT
PCDH20-/-

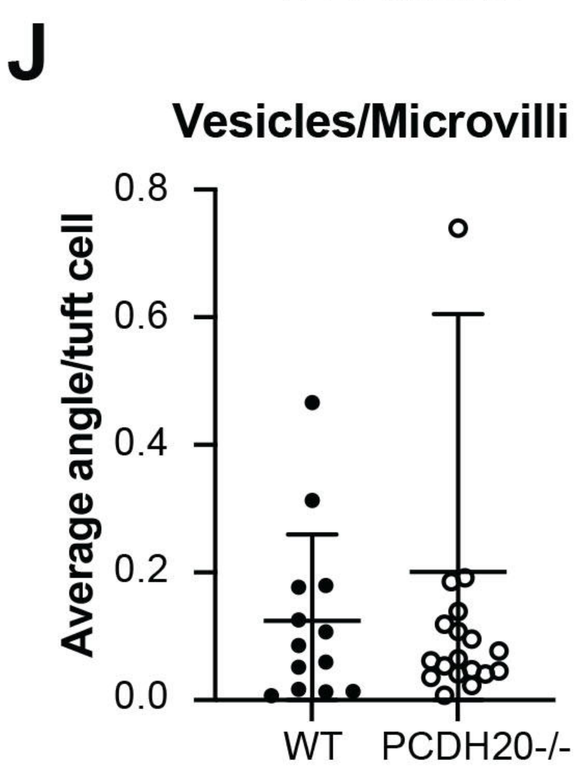
J
Vesicles/Microvilli
Average angle/tuft cell
0.8
0.6
0.4
0.2
0.0
WT
PCDH20-/-

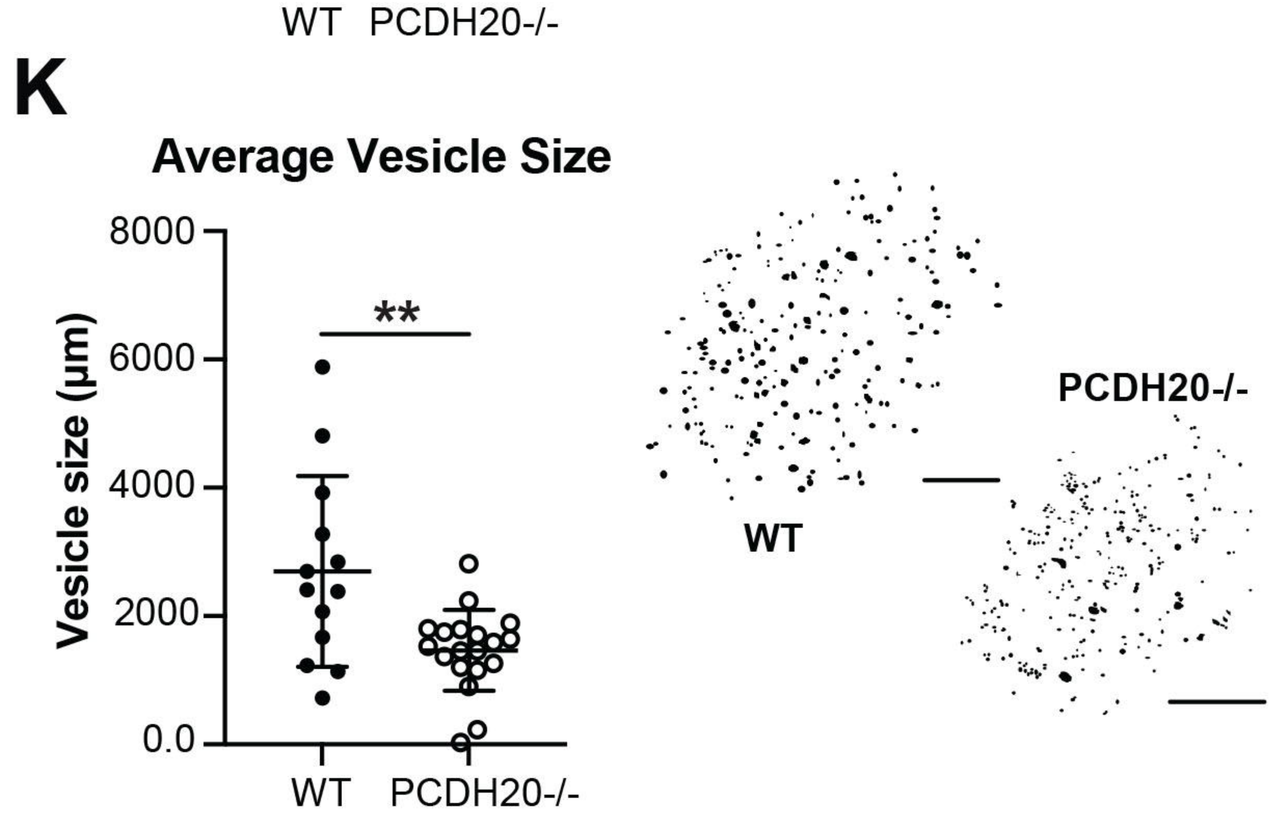
K
Average Vesicle Size
**
Vesicle size (µm)
8000
6000
4000
2000
0.0
WT
PCDH20-/-
PCDH20-/-
WT
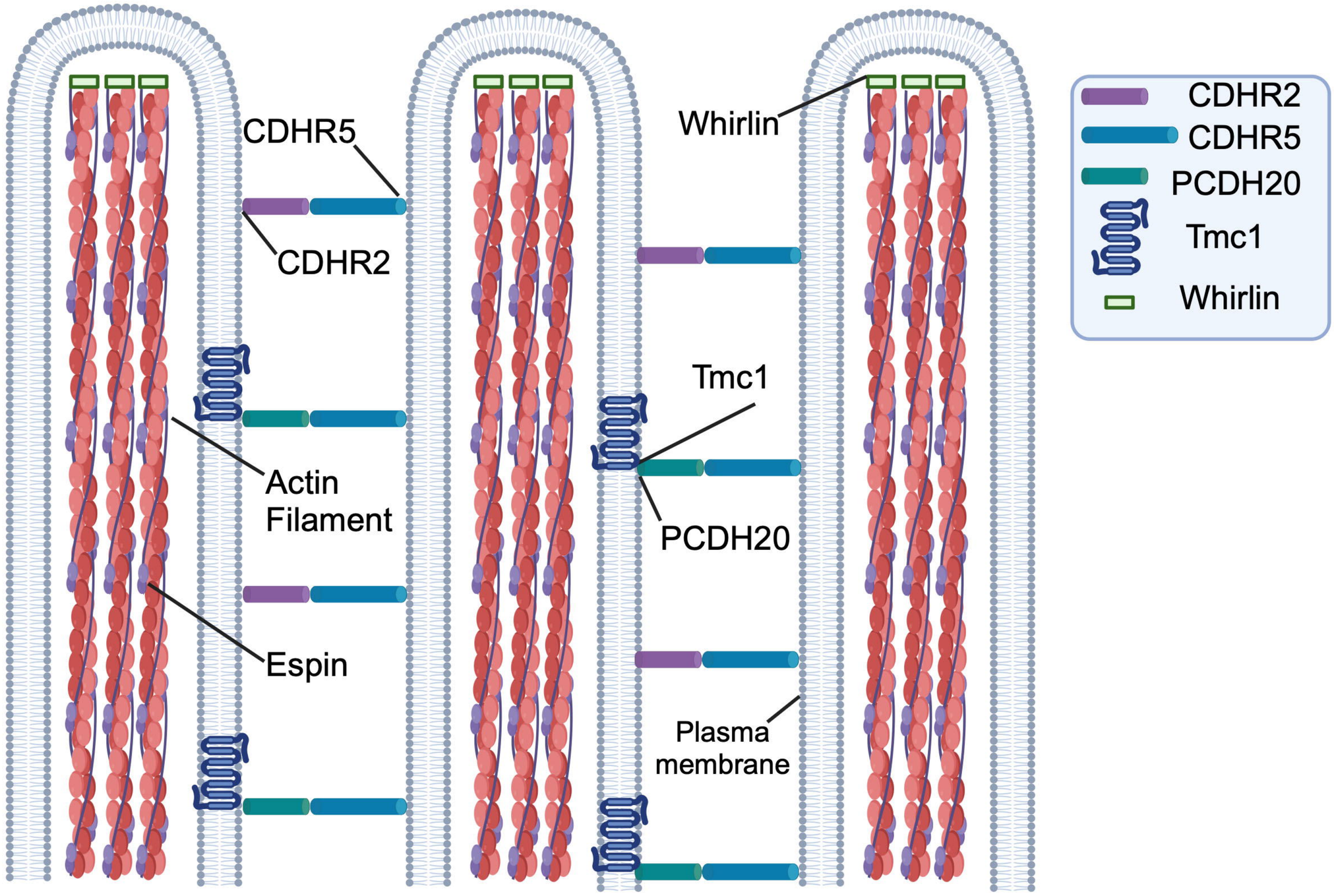
Tuft Cell Microvilli